

Extending the Turbidity Record—Making Additional Use of Continuous Data From Turbidity, Acoustic-Doppler, and Laser Diffraction Instruments and Suspended-Sediment Samples in the Colorado River in Grand Canyon

Scientific Investigations Report 2014–5097

FRONT COVER

View looking upstream on the Colorado River at the mouth of the tributary Paria River (center). The sediment-laden water of the Paria River enters and mixes with the clear Colorado River water released from Glen Canyon Dam (photograph by David Topping, May 17, 1993).

Extending the Turbidity Record—Making Additional Use of Continuous Data From Turbidity, Acoustic-Doppler, and Laser Diffraction Instruments and Suspended-Sediment Samples in the Colorado River in Grand Canyon

By Nicholas Voichick and David J. Topping

Scientific Investigations Report 2014–5097

**U.S. Department of the Interior
U.S. Geological Survey**

U.S. Department of the Interior
SALLY JEWELL, Secretary

U.S. Geological Survey
Suzette M. Kimball, Acting Director

U.S. Geological Survey, Reston, Virginia: 2014

For product and ordering information:
World Wide Web: <http://www.usgs.gov/pubprod>
Telephone: 1-888-ASK-USGS

For more information on the USGS—the Federal source for science about the Earth,
its natural and living resources, natural hazards, and the environment:
World Wide Web: <http://www.usgs.gov>
Telephone: 1-888-ASK-USGS (1-888-275-8747)

Any use of trade, firm, or product names is for descriptive purposes only and does not imply
endorsement by the U.S. Government.

Although this information product, for the most part, is in the public domain, it may also contain copyrighted materials
as noted in the text. Permission to reproduce copyrighted items must be secured from the copyright owner

Suggested citation:
Voichick, N., and Topping, D.J., 2014, Extending the turbidity record—making additional use of continuous data from
turbidity, acoustic-Doppler, and laser diffraction instruments and suspended-sediment samples in the Colorado River
in Grand Canyon: U.S. Geological Survey Scientific Investigations Report 2014–5097, 31 p., available online only at
<http://dx.doi.org/10.3133/sir20145097>.

ISSN 2328–0328 (online)

Contents

Acknowledgments	vi
Abstract	1
Introduction	1
Purpose and Scope	4
Background	5
Deployment of Instruments	6
Sediment Surrogates	7
Turbidity	7
Acoustic Attenuation and Backscatter	11
Comparing Different Types of Data	11
Acoustic Attenuation and Turbidity	11
Extending the Turbidity Record	13
Laser Diffraction and Transmission	17
Physical Explanation for Apparent Data Outliers	20
Conclusion	26
References Cited	28

Figures

1. Diagram showing the design components of a nephelometric turbidity instrument: the light source, the detector, and the optical geometry	2
2. Map of northwestern Arizona, showing the study area in Grand Canyon and the location of the monitoring stations	3
3. Graph showing the poor relation between the discharge of the Colorado River and suspended-sediment concentration at the CR030 monitoring station	8
4. Graphs showing relations between \log_{10} of turbidity and \log_{10} of total suspended-sediment concentration at the four monitoring stations downstream from Lees Ferry	9
5. Time series of turbidity of the Colorado River at the CR225 monitoring station during 5–10 August 2010	10
6. Graph showing theoretical variation in the 1-MHz acoustic sediment attenuation coefficient, relative to suspended-sediment concentration, compared against changing particle size	12
7. Graph showing relation between \log_{10} of turbidity and \log_{10} of suspended-sediment concentration of total sediment and of silt and clay alone at the CR087 monitoring station	12
8. Graphs showing relations between \log_{10} of acoustic sediment attenuation and \log_{10} of turbidity at three different frequencies at the CR087 monitoring station	13
9. Graphs showing turbidity over the periods of record at all monitoring stations in the study area	14
10. Graph of measured and estimated turbidity at the CR087 monitoring station from September 18 to 23, 2011	15
11. Box and whisker plots of turbidity during the period of record common to all five monitoring stations, January 29, 2008, through October 1, 2012	15

12. Graphs showing geometric daily mean turbidity at the CRLF and CR087 monitoring stations through the course of the year.....	16
13. Pre- and post-dam turbidity duration plots.....	16
14. Graphs showing relations between turbidity and LISST-100C-measured silt and clay concentration at the CR061 and CR087 monitoring stations	18
15. Graphs showing relations between sampled silt and clay concentration and LISST-100C-measured silt and clay concentration at the CR061 and CR087 monitoring stations compared with the relations between sampled silt and clay concentration and turbidity at the CR061 and CR087 monitoring stations.....	18
16. Graphs showing relations between turbidity and \log_{10} of laser transmittance measured using a LISST-100C laser-diffraction instrument at the CR061 monitoring station from June 20, 2005, through June 26, 2010, and the CR087 monitoring station from January 29, 2008, through June 15, 2010	19
17. Graph showing relation between turbidity and the 2-MHz acoustic sediment attenuation coefficient calculated from data collected using a 2-MHz Nortek EasyQ acoustic-Doppler profiler at the CR061 monitoring station	20
18. Graph showing relation between the 2-MHz acoustic sediment attenuation coefficient and silt and clay concentration at the CR061 monitoring station.....	21
19. Graph showing relation between the 1-MHz acoustic sediment attenuation coefficient and silt and clay concentration at the CR030 monitoring station.....	21
20. Graph showing relation between turbidity and silt and clay concentration at the CR061 monitoring station.....	21
21. Plots of grain-size distributions of suspended silt and clay from the CR031 and CR061 monitoring stations analyzed using a Beckman Coulter 13320 particle size analyzer and the pipet method	22
22. Graph showing the theoretical attenuation cross-section, which is the attenuation of light per unit mass of particles, caused by spherical quartz particles in suspension, as a function of their diameter.....	23
23. Graphs showing relations between the 1-MHz acoustic sediment attenuation coefficient and sediment concentration in different size classes at the CR030 monitoring station during "normal" dam releases, and the 2008 controlled-flood experiment	24
24. Photograph of sediment samples analyzed for grain-size distribution using the pipet method.....	25
25. Bar graph of clay mineral assemblages in suspended-sediment samples determined by x-ray diffraction.....	27

Tables

1. Monitoring stations (referenced in this study) for turbidity in the Colorado River, and turbidity probe types.....	4
2. Summary of turbidity measurements in river cross-sections in the vicinity of the monitoring stations and comparisons with concurrent turbidity readings taken at the monitoring stations	6
3. Summary of regression analysis of sediment concentration as a function of turbidity at the four monitoring stations below the CRLF station.....	9
4. Summary of turbidity statistics over the periods of record for all monitoring stations.....	10

Conversion Factors

Inch/Pound to SI

Multiply	By	To obtain
Length		
inch (in.)	25,400,000	nanometer (nm)
inch (in.)	25,400	micron (μm)
inch (in.)	25.4	millimeter (mm)
foot (ft)	0.3048	meter (m)
mile (mi)	1.609	kilometer (km)
Volume		
ounce, fluid (fl oz.)	29,570	microliter (μl)
ounce, fluid (fl oz.)	0.02957	liter (L)
pint (pt)	0.4732	liter (L)
quart (qt)	0.9464	liter (L)
gallon (gal)	3.785	liter (L)
Flow rate		
cubic foot per second (ft^3/s)	0.02832	cubic meter per second (m^3/s)
Mass		
ounce, avoirdupois (oz)	28.35	gram (g)

SI to Inch/Pound

Multiply	By	To obtain
Length		
nanometer (nm)	0.00000003937	inch (in.)
micron (μm)	0.00003937	inch (in.)
millimeter (mm)	0.03937	inch (in.)
meter (m)	3.281	foot (ft)
kilometer (km)	0.6214	mile (mi)
Volume		
microliter (μl)	0.00003381	ounce, fluid (fl. oz)
liter (L)	33.81	ounce, fluid (fl. oz)
liter (L)	2.113	pint (pt)
liter (L)	1.057	quart (qt)
liter (L)	0.2642	gallon (gal)
Flow rate		
cubic meter per second (m^3/s)	35.31	cubic foot per second (ft^3/s)
Mass		
gram (g)	0.03527	ounce, avoirdupois (oz)

Acknowledgments

This research was funded by the U.S. Department of the Interior's Glen Canyon Dam Adaptive Management Program through the USGS Grand Canyon Monitoring and Research Center. Tom Sabol, Ron Griffiths, Karen Vanaman, Robert Tusso, and both of the authors all participated in the collection of data and maintenance of equipment. Pete Weiss, Stuart Reeder, Steve Jones, J.P. Running, and Brian Dierker provided technical boating support and also participated in the collection of data. Giovanni Prestigiacomo of Beckman Coulter Incorporated provided grain-size analyses of suspended-sediment samples. Expertise on X-ray diffraction procedures and analysis of results was provided by Roderic Parnell, Northern Arizona University. Thoughtful reviews that greatly improved this manuscript were provided by Chauncey Anderson, Mike Sadar, and Chris Gippel.

Extending the Turbidity Record—Making Additional Use of Continuous Data From Turbidity, Acoustic-Doppler, and Laser Diffraction Instruments and Suspended-Sediment Samples in the Colorado River in Grand Canyon

By Nicholas Voichick and David J. Topping

Abstract

Turbidity is a measure of the scattering and absorption of light in water, which in rivers is primarily caused by particles, usually sediment, suspended in the water. Turbidity varies significantly with differences in the design of the instrument measuring turbidity, a point that is illustrated in this study by side-by-side comparisons of two different models of instruments. Turbidity also varies with changes in the physical parameters of the particles in the water, such as concentration, grain size, grain shape, and color. A turbidity instrument that is commonly used for continuous monitoring of rivers has a light source in the near-infrared range (860±30 nanometers) and a detector oriented 90 degrees from the incident light path. This type of optical turbidity instrument has a limited measurement range (depending on pathlength) that is unable to capture the high turbidity levels of rivers that carry high suspended-sediment loads. The Colorado River in Grand Canyon is one such river, in which approximately 60 percent of the range in suspended-sediment concentration during the study period had unmeasurable turbidity using this type of optical instrument. Although some optical turbidimeters using backscatter or other techniques can measure higher concentrations of suspended sediment than the models used in this study, the maximum turbidity measurable using these other turbidimeters may still be exceeded in conditions of especially high concentrations of suspended silt and clay. In Grand Canyon, the existing optical turbidity instruments remain in use in part to provide consistency over time as new techniques are investigated. As a result, during these periods of high suspended-sediment concentration, turbidity values that could not be measured with the optical turbidity instruments were instead estimated from concurrent acoustic attenuation data collected using side-looking acoustic-Doppler profiler (ADP) instruments. Extending the turbidity record to the full range of sediment concentrations in the study area using data from the ADP instruments is particularly useful for biological studies. In Grand Canyon, turbidity has been correlated with food availability for aquatic organisms (gross primary production) as well as with fish behavior specific to predator-prey interactions. On the basis of the complete “extended” turbidity record

and the relation between suspended-sediment concentration and turbidity, levels were higher before the construction of Glen Canyon Dam by a factor of approximately 2,000 at the Lees Ferry monitoring station (15 miles downstream from the dam) and by a factor of approximately 20 at the monitoring station 87 miles downstream from Lees Ferry (102 miles downstream from the dam). A comparison of turbidity data with data from Laser In-Situ Scattering and Transmissometry (LISST) laser-diffraction instruments, suspended-sediment concentration data, and ADP data shows the influence of the physical properties of suspended sediment. Apparent outliers in relations between turbidity, ADP, and suspended-sediment data during two events within the study period, a 2007 tributary flood from a watershed altered by a recent wildfire and a 2008 experimental controlled-flood release from Glen Canyon Dam, are explained in part by atypical grain sizes, shapes, densities, colors, and (or) clay mineral assemblages of suspended sediment occurring in the Colorado River during these two events. These analyses demonstrate the value of using multiple data-collection strategies for turbidity and sediment-transport studies and of continuous monitoring for capturing the full range and duration of turbidity and sediment-transport conditions, identifying the provenance of the sediment causing turbidity, and detecting physical and chemical processes that may be important for management of critical physical and biological resources.

Introduction

Measurement of turbidity in rivers is often portrayed and monitored as a direct measurement of water clarity, when it is actually an expression of the scattering and absorption of light in water rather than the transmission of light in a straight line (American Public Health Association and others, 2005). This is an important distinction, because turbidity is an instrument-specific measurement dependent on the design of the instrument as well as the optical character of the particles in the water. There are three design components that dictate the response of a turbidity instrument: the light source, the detector(s), and the optical geometry, which includes the path

2 Extending the Turbidity Record—Using Continuous Instrument Data and Suspended-Sediment Samples

length of the light and the angle of the detector(s) from the incident light path (fig. 1; Hach and others, 1985). Additional factors, such as proprietary postprocessing algorithms and calibration techniques, can also influence turbidity readings. The turbidity instruments used in the Grand Canyon study described in this paper, and commonly used in other research and monitoring studies, have a single light source in the near-infrared range (860 ± 30 nanometers) and a single detector oriented 90 degrees from the incident light path. Turbidity measured by these instruments should be reported in Formazin Nephelometric Units (FNU), because the units of measurement of turbidity define the type of instrument that was used to collect the readings (ASTM International, 2011).

The scattering of light, and thus the measured turbidity, is affected by suspended and dissolved matter, such as clay, silt, sand, finely divided organic and inorganic matter, soluble colored organic compounds, and plankton and other microscopic organisms (American Public Health Association and others, 2005). In most natural waters, including in the Colorado River in Grand Canyon, the scattering of light is dominated by particles (Kirk, 1985). Turbidity is affected by the characteristics of the particles, including concentration, grain size, grain shape, refractive index, and color of the particles and of the dissolved matrix (Sadar, 1998). Turbidity instruments are, in most cases, calibrated using a formazin polymer (tetraformal trisazine [TFTA]; Schmidt, 1984) as the primary reference standard, or using a standard that has been controlled against formazin. Even though all makes and models of optical turbidity instruments are calibrated to the same standard, they may react differently to the same environmental sample; turbidity measurements of the same environmental sample using instruments with different design components can vary by a factor of 2 or more (Anderson, 2005). For this reason, consistency of instrument types and techniques is one of the most important

considerations in a turbidity monitoring program (Anderson, 2005). Cross-calibration based on side-by-side comparison of turbidity measurements made with different model instruments is required before measurements made with different model instruments can be compared at a particular study site. Thus, when different model instruments are used in different rivers, the utility of turbidity for quantitative comparison of water-clarity conditions between different river systems can be limited. However, when instrumentation is consistent, turbidity has several useful applications.

Under certain conditions, turbidity has been successfully used as a surrogate for suspended-sediment concentration (Lewis, 1996; Finlayson, 1985; Christensen and others, 2002; Rasmussen and others, 2009). Environmental management of rivers often requires the construction and analysis of accurate sediment budgets (for example, Grams and Schmidt, 2005; Topping and others, 2010). Because discharge of water and suspended-sediment concentration are poorly correlated in many rivers (for example, Gray and Simoes, 2008), accurate sediment budgets require a large number of suspended-sediment measurements. Unfortunately, making the large number of suspended-sediment measurements required for accurate sediment records can be cost and labor prohibitive. In rivers that have fairly consistent suspended-sediment characteristics dominated by relatively low concentrations of silt and clay, continuously recording optical turbidity instruments have been successfully used to make surrogate measurements of suspended-sediment concentration, vastly improving the sediment record and reducing the frequency of time-consuming and expensive conventional suspended-sediment sampling (Finlayson, 1985; Christensen and others, 2002; Rasmussen and others, 2009).

Turbidity has also been related to the behavior of sight-feeding fishes and their prey (Gregory, 1993; Abrahams and

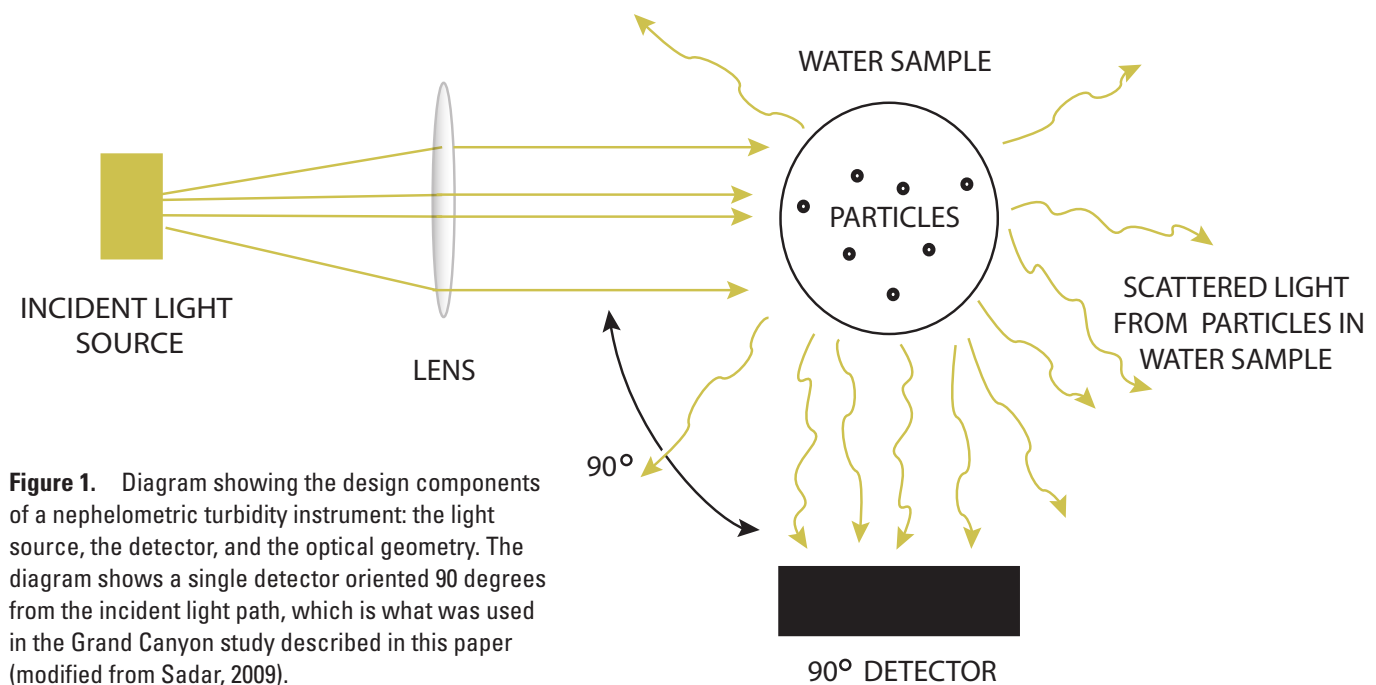


Figure 1. Diagram showing the design components of a nephelometric turbidity instrument: the light source, the detector, and the optical geometry. The diagram shows a single detector oriented 90 degrees from the incident light path, which is what was used in the Grand Canyon study described in this paper (modified from Sadar, 2009).

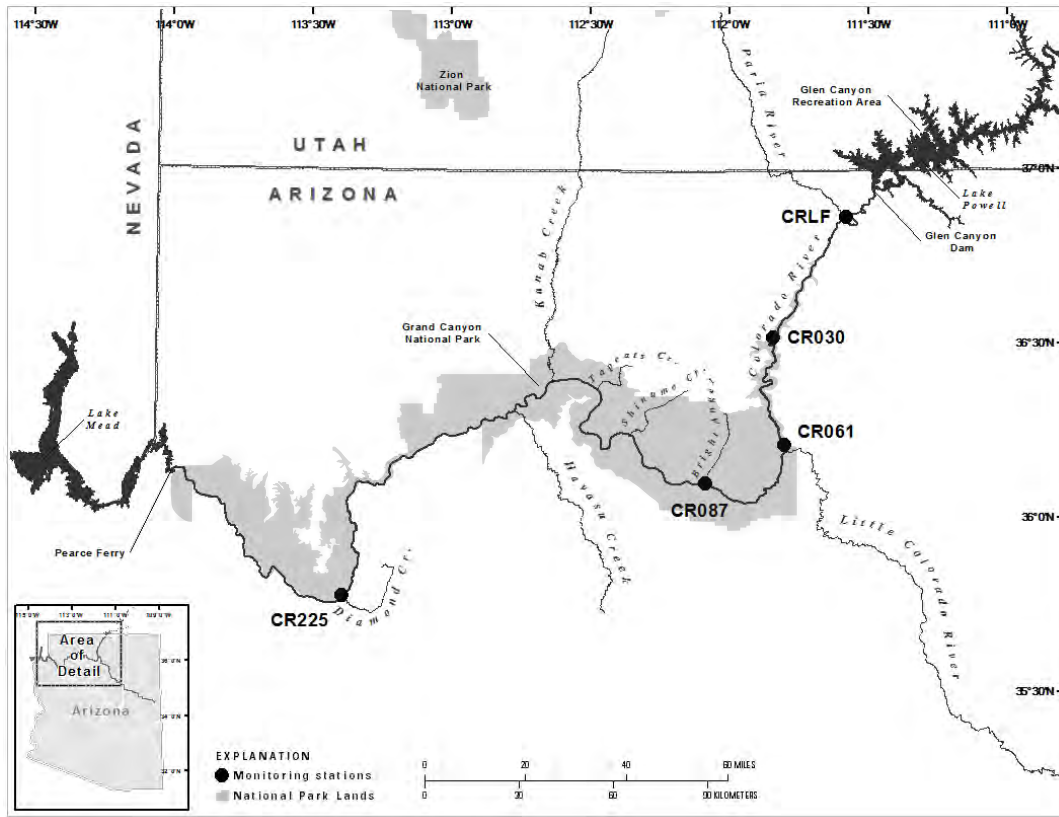


Figure 2. Map of northwestern Arizona, showing the study area in Grand Canyon and the location of the monitoring stations described in this paper (refer to table 1 for station names).

Kattenfeld, 1997; Stone, 2010; Yard and others, 2011). A trout piscivory study conducted on the Colorado River in Grand Canyon, near the confluence with the Little Colorado River (fig. 2), suggests that increasing turbidity reduces the visual detection of prey fish. However, this reduction in the visual detection of prey fish may be mediated by (1) a shift in feeding behavior of the rainbow trout from drift feeding to active feeding on fish and (or) (2) the increased availability of the prey fish (Yard and others, 2011). Yard and others (2011) related suspended-sediment concentration, rather than turbidity, to fish behavior, because the turbidity record was incomplete during their study period. Suspended-sediment concentration was thought to influence fish behavior primarily because of its optical effect on water clarity. The optical properties of suspended sediment are strongly dependent on the grain-size distribution; silt-and-clay-sized sediment affects water clarity conditions much more than larger (sand-sized) sediment (Davies-Colley and others, 1993). Thus, because the grain-size distribution of suspended sediment varies substantially in the study area (see, for example, Topping and others, 2000a, 2000b, 2010) and different grain-size distributions give rise to very different levels of turbidity at identical suspended-sediment concentrations, it is preferable to relate fish feeding behavior directly to an optical measurement, such as turbidity, than just to suspended-sediment concentration. Stone (2010) related fish behavior on the Little Colorado River (fig. 2) directly to turbidity. He established species-specific turbidity

thresholds, above which particular species of fish are much less likely to enter a hoop net. Stone hypothesized that the effects of changes in visual clarity reflect a behavioral switch by many fishes, from relying primarily on physical cover, such as hoop nets, in clear water conditions, to using conditions of low visual clarity as cover to reduce the predation risks (Stone, 2010; Gregory, 1993).

A drawback of optical turbidity instruments is that the upper limit of recordable turbidity is determined by the instrument's maximum recording level. Optical turbidity instruments that record in Formazin Nephelometric Units (fig. 1), which are commonly used for river research, have path lengths that in many cases result in a maximum recording level somewhere in the range of approximately 1,000 to 1,500 FNU¹. As noted, the suspended-sediment concentration

¹ There are turbidity instruments that are capable of measuring higher turbidity levels than the instruments used in this study. Instruments with different design components (for example instruments with shorter pathlengths, or backscatter instruments) are capable of detecting turbidity values greater than 10,000 units. However, instruments utilizing the alternative technologies capable of measuring higher levels of turbidity are not always able to accurately measure low turbidity levels (ASTM International, 2011). Nor are the instruments utilizing these alternative technologies capable of measuring the highest turbidity levels observed in this study. The turbidity instruments used in the study area were therefore chosen because they (1) could be deployed economically with existing multiparameter water-quality instruments and (2) they were capable of accurately detecting low turbidity levels, important for monitoring biological activity in the study area.

4 Extending the Turbidity Record—Using Continuous Instrument Data and Suspended-Sediment Samples

corresponding to the maximum recording level of the turbidity probe will vary depending on the grain-size distribution and, to a lesser degree, on other physical factors. In the Colorado River in Grand Canyon, a value of 1,200 FNU corresponds to a suspended-sediment concentration of approximately 1,500 to 2,000 mg/L under typical conditions, when most of the suspended sediment is composed of silt-and-clay-sized sediment, but will correspond to higher suspended-sediment concentrations (approximately 6,500 to 7,500 mg/L) when most of the suspended sediment is composed of sand-sized sediment (based on analyses done in this study). Although many rivers in the United States have turbidity levels that rarely approach the instrument's maximum recording level, many rivers in the western United States can have sediment concentrations much greater than the maximum recording level of turbidity probes, including the Colorado River and its tributaries in Colorado, Utah, and Arizona (>100,000 mg/L), the Rio Grande and its tributaries in New Mexico and Texas (>30,000 mg/L), and the Powder River in Wyoming (>100,000 mg/L) (data from U.S. Geological Survey National Water Information System and Grand Canyon Monitoring and Research Center databases). In this study, we extend turbidity above the optical instrument's maximum recording level through use of measurements of acoustic attenuation, allowing for the calculation of complete daily, seasonal, and annual turbidity statistics and enabling biologists to accurately determine both thresholds and durations of turbidity important for governing fish behavior and controlling gross primary productivity.

Purpose and Scope

The purpose of this report is to analyze turbidity, suspended-sediment, acoustic-attenuation, laser-transmission, and laser-diffraction data to (1) determine whether such data can be used to extend the range of measurable turbidity,

(2) estimate changes in optical clarity before and after the construction of Glen Canyon Dam, and (3) provide insight as to the cause of apparent data outliers from anomalous events leading to unusual turbidity characteristics. This report describes methods to extend the optically measured turbidity record in two ways. First, the turbidity record is extended to the full range of visual clarity using acoustic-attenuation data. Second, the turbidity record is also “extended” to result in new knowledge by using turbidity, suspended-sediment, acoustic-attenuation, laser-transmission, and laser-diffraction data together to identify atypical suspended-sediment properties that allowed us to infer the provenance of sediment that led to unusual turbidity characteristics.

The extension of these data and their use in distinguishing sediment sources and characteristics are demonstrated using two distinct events that occurred during the study period. The first event, a March 2008 controlled-flood experiment, was conducted when the discharge from Glen Canyon Dam was increased to 42,000 cubic feet per second, almost three to four times the average discharge, for approximately 60 hours (Schmidt and Grams, 2011a). This controlled-flood experiment resulted in a coarsening of suspended sediment that primarily originated from sediment stored in the river bed (rather than being supplied by an upstream tributary). During the 2008 controlled-flood experiment, the suspended silt and clay was almost entirely composed of silt-sized sediment, as opposed to a predominance of clay-sized particles, which is common under typical flows. The second event was the result of a large flood on July 23, 2007, that originated in an ephemeral stream that enters the Colorado River approximately 17 miles downstream from the Colorado River at Lees Ferry (CRLF) station and 13 miles upstream from the Colorado River near river mile 30 (CR030) station (fig. 2, table 1). Both of these events resulted in outliers on the turbidity/acoustic-sediment-attenuation-coefficient plots at multiple downstream stations, with data collected from multiple instruments.

Table 1. Monitoring stations (referenced in this study) for turbidity in the Colorado River, and turbidity probe types.

[River miles are distances downstream from Lees Ferry; Glen Canyon Dam is 15 miles upstream from Lees Ferry]

Station name (position relative to Paria River and Little Colorado River)	Station identifier	Period of turbidity record	Date of Switch from YSI 6026 to 6136 turbidity probe
Colorado River at Lees Ferry, Arizona, USGS gaging station 09380000 (located above Paria River)	CRLF	Dec. 21, 2005–Oct. 1, 2012	All data 6136 probe
Colorado River near river mile 30 (located between Paria River and Little Colorado River)	CR030	May 28, 2005–Oct. 1, 2012	Mar. 21, 2006
Colorado River near river mile 61 (located between Paria River and Little Colorado River)	CR061	May 30, 2005–Oct 1, 2012	Sep. 28, 2005
Colorado River near Grand Canyon, Arizona, USGS gaging station 09402500 (located near river mile 87 below Little Colorado River)	CR087	Jan. 29, 2008–Oct. 1, 2012	All data 6136 probe
Colorado River above Diamond Creek near Peach Springs, Arizona, USGS gaging station 09404200 (located near river mile 225 below Little Colorado River)	CR225	Feb. 15, 2006–Oct. 1, 2012	All data 6136 probe

Background

The completion of Glen Canyon Dam in 1963 resulted in an approximately 95-percent reduction of the sediment supply to the Colorado River at the upstream boundary of Grand Canyon National Park (Topping and others, 2000a). This reduced sediment supply has resulted in a relatively clear river, but the humpback chub, a federally listed endangered native fish species that evolved in a highly turbid river, persists and is the focus of substantial management concern (Gorman and Stone, 1999). Monitoring of turbidity and other water-quality parameters occurs at the CRLF station and at four additional stations located farther downstream (fig. 2, table 1). Monitoring of sediment transport occurs at all stations in this study except the CRLF station. Two purposes of conducting the monitoring are (1) to inform managers of how various flow regimes affect the quantity and location of sand bars and other fine-sediment deposits in Grand Canyon and the availability of sediment that could be utilized to rebuild sand bars and (2) to provide data to biologists for determining relations among suspended sediment, water quality, and food availability for fish, as well as fish habitat, behavior, and survival. In addition to turbidity, the water quality data collected at the monitoring stations include water temperature (Voichick and Wright, 2007; Wright and others, 2008), specific conductance (Voichick, 2008; Voichick and Topping, 2010), and dissolved oxygen (these data are available online at http://www.gcmrc.gov/discharge_qw_sediment/stations/GCDAMP).

Management of the Colorado River downstream from Glen Canyon Dam requires accurate sediment budgets, and construction of these sediment budgets requires accurate knowledge of sediment loads bracketing key reaches within Grand Canyon (Schmidt and Grams, 2011a, 2011b; Topping and others, 2010). Sediment loads are the product of discharge and suspended-sediment concentration. Hence, accurate determination of sediment loads requires knowing both discharge and suspended-sediment concentration frequently, and these two parameters vary nonrandomly and independently from each other (Porterfield, 1972; Gray and Simoes, 2008). Because the correlation between discharge and suspended-sediment concentration is poor in the Colorado River in Grand Canyon (Topping and others, 2000a, 2000b), discharge cannot be used as a proxy for suspended-sediment concentration. Therefore, sediment-rating curves, based on regressions between discharge and suspended-sediment concentration, cannot be used, and suspended-sediment concentrations must be measured at intervals shorter than the discharge-independent variation in suspended-sediment concentration driven by changes in the upstream sediment supply. The intervals over which suspended-sand concentrations and suspended-silt-and-clay concentrations have been observed to vary independently of discharge in the Colorado River (as a result of upstream tributary flooding and sustained high dam releases) can be much less than 1 hour (Topping and others, 2000a, 2000b). Thus, an appropriate interval at which to measure discharge,

suspended-sediment concentration, and turbidity in the Colorado River in Grand Canyon is 15 minutes.

As in most rivers, discharge in the Colorado River is measured by the U.S. Geological Survey (USGS) using the more easily measured parameter “stage” as a proxy (Rantz and others, 1982). Because discharge cannot be used as a proxy for suspended-sediment concentration in the Colorado River and it is impossible to measure suspended-sediment concentration at 15-minute intervals using only the conventional sediment-sampling methods described in Edwards and Glysson (1999), sediment surrogate technologies have been pursued to make high-temporal-resolution measurements of suspended-sediment concentrations and grain-size distributions in the Colorado River in Grand Canyon (Melis and others, 2003; Topping and others, 2004, 2006, 2007, 2010). The sediment-transport monitoring network for the Colorado River in Grand Canyon that utilizes these surrogate technologies is described in Griffiths and others (2012). Direct measurements of suspended-sediment concentration and grain size are made episodically in the study area using the Equal-Discharge-Increment (EDI), Equal-Width-Increment (EWI), and automatic-pump methods described in Edwards and Glysson (1999). Surrogate measurements of suspended-sediment concentration and grain size are made in the study area at a 15-minute interval using three types of instruments: acoustic-Doppler profilers (ADP) at multiple frequencies, Laser In-Situ Scattering and Transmissometry (LISST) laser-diffraction instruments, and optical turbidity probes. The EDI and EWI measurements are used to calibrate and subsequently verify the sediment measurements made using the automatic-pump samplers and surrogate technologies (Griffiths and others, 2012). The wealth of different types of data collected at the monitoring stations against which turbidity can be compared (that is, ADP, LISST, and suspended sediment) makes the Colorado River in Grand Canyon the ideal study area to evaluate the different physical controls on turbidity.

The silt and clay in the Colorado River in Grand Canyon typically has consistent physical properties, namely grain size, color, shape, clay-mineral content, and refractive index, because most of these finer grained sediments (as well as the coarser sand-sized sediment) originate from flooding events on only two tributaries, the Paria River and the Little Colorado River (fig. 2). Clay from both of these tributaries is dominated by montmorillonite (in the smectite group), illite, and kaolinite (Beverage and Culbertson, 1964). This study investigates the degree to which the silt-and-clay baseline conditions set by these two major tributaries vary compared with those of sediment supplied by experimental controlled-flood releases from Glen Canyon Dam and during relatively infrequent floods on tributaries with different or changing sediment properties. The ADP, laser diffraction instruments, and turbidity sensors each respond differently to the physical parameters of the sediment. By comparing the data from these instruments, and including additional data obtained from suspended-sediment samples (concentration and grain-size distribution),

suspended sediment with unusual physical properties (such as atypical grain size, shape, or mineral content) can therefore be identified.

Deployment of Instruments

The water-quality instruments used to measure turbidity were also used to concurrently measure temperature, specific conductance, and dissolved oxygen (Voichick and Wright, 2007; Voichick, 2008; Voichick and Topping, 2010). The instruments, manufactured by YSI Incorporated, were suspended in the river at or near the river bank, except at the CRLF monitoring station, where the instrument was originally suspended from a mid-channel buoy.

Additional instruments deployed at the stations were ADPs (at all four stations downstream from the CRLF station) and LISST instruments at the CR061 and CR087 stations. All instruments were set up to record either instantaneous or time-averaged values at a 15-minute interval. The instruments were serviced at intervals of 1 to 4 months; the more accessible stations (CR087 and CR225) were serviced more frequently (approximately monthly), and the more remote stations (CR030 and CR061) were serviced less frequently (generally every 3 to 4 months). During servicing of the water-quality instruments, protocols described in Wagner and others (2006) were followed: a field meter was installed, the turbidity probes were cleaned (wiper pads replaced when necessary) and then redeployed to check for biological fouling, after which a turbidity calibration check was performed (using 0 and 1,000 FNU standards). All the turbidity probes used in the study area were equipped with mechanical wipers to reduce biological fouling. At all stations except CRLF, instruments were powered by onshore batteries charged by solar panels. Late in the study, the water-quality instruments at the CRLF station were

redployed near the bank and powered by onshore batteries charged by solar panels because of ongoing maintenance and data-loss issues. Two-way remote communication with the instruments via satellite was set up at all stations except CRLF and CR225. Data from the instruments were downloaded from the office (or the field during servicing) approximately every month, and the instruments could be programmed from the office when necessary. Late in this study, data from the instrument at the CRLF station could be downloaded via satellite using the GOES system at the USGS Colorado River at Lees Ferry, Arizona, gaging station (09380000).

To check whether the turbidity measurements at the nearshore deployments were representative of the average turbidity in the river cross section, cross-section measurements were taken in the vicinity of each station during conditions of varying turbidity (table 2). During the cross-section measurements, turbidity was recorded at five locations across the river channel while concurrent turbidity measurements were made at the permanently deployed nearshore station (Wagner and others, 2006). At each of the five locations, a vertical profile of turbidity was measured from the water surface to near the channel bottom in 5-foot increments. The cross-section results showed that for turbidity less than 10 Formazin Nephelometric Units (FNU; Anderson, 2005), the cross-section readings were often higher than from the deployed field meter by as much as 26 percent (table 2). However there is significant variability between the cross-section and site readings at low turbidity (table 2), probably representing higher uncertainty at turbidity levels less than 10 FNU. For higher turbidity levels (greater than 20 FNU), there was less than a 5-percent difference between turbidity at the nearshore location and the cross-section readings.

In the study area, two models of turbidity probes, both manufactured by YSI Incorporated, were used, model 6026 and model 6136 (table 1). The model 6136 turbidity

Table 2. Summary of turbidity measurements in river cross-sections in the vicinity of the monitoring stations and comparisons with concurrent turbidity readings taken at the monitoring stations (at the long-term deployment sites near the river bank).

Date	Station identifier	Average cross-section reading (Formazin Nephelometric Units)	Percent difference between cross-section reading and site reading (positive value indicates higher cross-section reading than site reading)
August 2009	CR030	5	-6
August 2007	CR030	7	14
February 2010	CR030	37	3
August 2010	CR030	272	-5
August 2009	CR061	8	26
August 2010	CR061	27	2
February 2010	CR061	81	0
August 2007	CR061	403	-1
August 2009	CR087	7	23
February 2010	CR087	31	4
May 2010	CR225	20	13
September 2010	CR225	278	3

instrument used the same light-source wavelength and detection angle as the older model 6026 instrument, but the optics were altered, in part to improve results at low turbidity levels (YSI Incorporated, 2002). This change in optics resulted in a substantial difference in the turbidity readings of the same environmental sample using the two models of probes. Based on side-by-side measurements of the two models of turbidity probes in a Kansas stream, YSI recommended converting the 6026 readings into an equivalent 6136 reading using

$$y = 0.6486x, \quad (1)$$

where x is the model 6026 turbidity-probe value and y is the model 6136 turbidity-probe value (YSI Incorporated, 2005). To see if this equation held for Grand Canyon, a side-by-side comparison of the two models of probes was conducted at both the CR030 and CR061 monitoring stations (table 1). These comparisons, which were conducted over an 8-month period at a 15-minute sampling frequency, included turbidity values covering close to the full reporting range of the probes. During the comparison, model 6136 turbidity-probe values ranged from approximately 1 to 900 FNU at the CR030 station and from 0.5 to 1,200 FNU at the CR061 station. The probe comparisons yielded the following relations: for the CR030 station,

$$y = 0.495x, \quad (2)$$

and for the CR061 station,

$$y = 0.633x. \quad (3)$$

The factor-of-two difference in the relations between turbidity measured with the two probe models, and the difference in the relations between the Kansas river and Colorado River in Grand Canyon and between the two stations on the Colorado River in the study area, illustrates that the measured turbidity value is dependent on both the design components of the instrument and the characteristics of the sediment in the water. Thus, when turbidity probes are changed from one model to another, side-by-side comparisons must be conducted at the locations where these probes are deployed; calibration relations developed on the basis of side-by-side comparisons conducted at locations other than the deployment location may be incorrect, giving rise to potentially large biases.

Sediment Surrogates

The USGS approach for monitoring suspended sediment in rivers traditionally has been to collect isokinetic velocity-weighted samples from the river cross-section using either

the EDI or EWI methods (Edwards and Glysson, 1999) and then to calculate sediment loads using the methods described in Porterfield (1972). Other sediment samples collected using alternative methods, such as single-vertical or pump samples, are calibrated to the velocity-weighted depth-integrated, cross-sectional samples. A suspended-sediment concentration curve is then developed by interpolating between measured suspended-sediment concentration values and is combined with the water-discharge curve to calculate daily suspended-sediment discharge (Porterfield, 1972; Gray and Simoes, 2008). During times when suspended-sediment data are scarce but water discharge is known, a less accurate estimate of suspended-sediment load is sometimes calculated from the empirical relation between water discharge and suspended-sediment concentration known as a sediment-rating curve (Porterfield, 1972; Gray and Simoes, 2008). The sediment-rating curve approach cannot be used in the Colorado River in Grand Canyon, because discharge of water and suspended-sediment concentration are poorly correlated (fig. 3). This situation exists because tributaries provide all of the sediment while accounting for only a fraction of the discharge of the Colorado River in Grand Canyon. Furthermore, the timing of sediment-supplying events in the tributaries and high-discharge events in the Colorado River is not correlated (Topping and others, 2000b). Thus, calculation of sediment loads in the Colorado River in Grand Canyon requires collection of suspended-sediment data at intervals shorter than the timescales over which discharge and suspended-sediment concentration vary independently from each other (that is $\ll 1$ hour). Using a surrogate for suspended-sediment concentration is especially appealing in rivers such as the Colorado River in Grand Canyon, where suspended-sediment concentration and grain size both vary substantially, systematically, and somewhat independently of water discharge (Topping and others, 2000a, 2000b).

Turbidity

Turbidity has been successfully used to estimate suspended-sediment concentration and load at a number of sites that have accurate discharge records and a highly correlated relation between turbidity and suspended-sediment concentration (Lewis, 1996; Finlayson, 1985; Christensen and others, 2002; Rasmussen and others, 2009). The USGS has established guidelines for using turbidity as a surrogate for suspended-sediment concentration in streams (Blanchard and Schertz, 2009; Rasmussen and others, 2009). These guidelines suggest developing a simple linear regression (SLR) model using turbidity and suspended-sediment concentration (SSC) data collected using approved USGS methods (Wagner and others, 2006; Edwards and Glysson, 1999). According to the guidelines, the model standard percentage error (MSPE, root-mean-squared error expressed as a percentage) of the SLR should be less than 20 percent (Rasmussen and others, 2009). In the present study, an evaluation was first made to determine whether log transformation of the data was warranted;

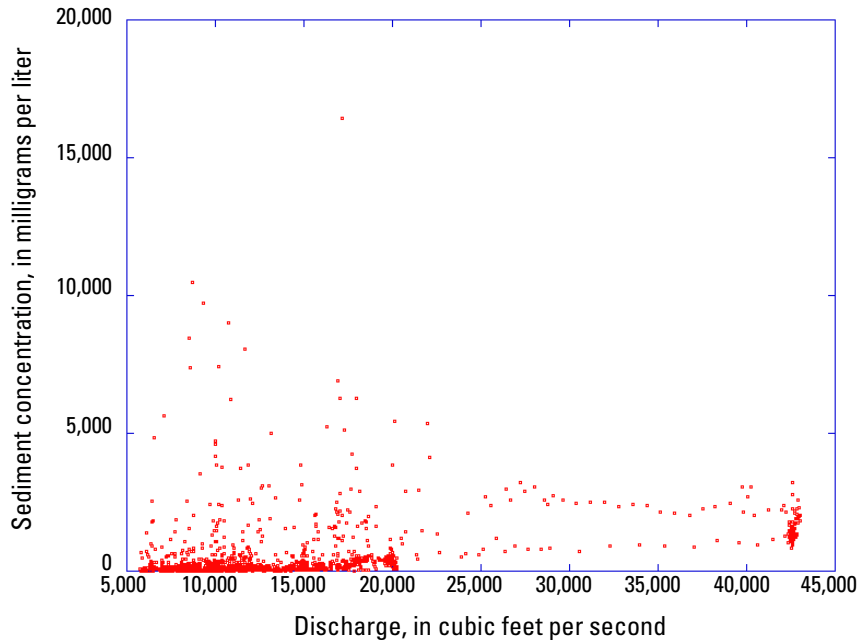


Figure 3. Graph showing the poor relation between the discharge of the Colorado River and suspended-sediment concentration at the CR030 monitoring station from July 2002 through November 2010.

Breusch-Pagan tests for heteroscedasticity (the dependence of the estimated variance of the residuals from a regression on the values of the independent variables) were therefore performed on the linear and \log_{10} -transformed turbidity and suspended-sediment data at the four monitoring stations downstream from Lees Ferry (table 3; Breusch and Pagan, 1979). In these tests, turbidity was the independent variable and suspended-sediment concentration was the dependent variable; thus, the Breusch-Pagan tests were conducted on the square of the residuals in linear and \log_{10} -transformed sediment concentration. Suspended sediment was represented as both total sediment (sand, silt, and clay) and only silt and clay (by separating the silt and clay from the sand-sized grains in the laboratory) using samples collected with EDI and EWI methods (the pump samples were not included). Silt and clay was regressed separately from total sediment, because silt-and-clay-sized particles contribute substantially more to turbidity than sand-sized particles (Davies-Colley and others, 1993). Residual plots were also analyzed visually to further assess whether log transformation reduced (1) the existence of data curvature relative to the regression model or (2) the heteroscedasticity of the data (table 3; Helsel and Hirsch, 2002). It is generally preferable to maintain the same type of model throughout a study area (Helsel and Hirsch, 2002) and, based on these analyses, \log_{10} transformation of the turbidity and suspended-sediment data at all stations in the study area was justified.

A likely explanation for the relatively high MSPE in the study area (fig. 4) is that the physical properties of the suspended sediment vary considerably. The correlation between turbidity and the suspended-sediment concentration depends on how much the light scattering and absorptive properties of the sediment vary during a single storm event and between storm events (Gippel, 1989). A high correlation between turbidity and suspended-sediment concentration is expected

when the physical properties of the sediment do not vary significantly as the concentration varies (Gippel, 1989). In the sediment-supply-limited conditions in Grand Canyon, the sand on the bed and in suspension is (in most cases) finer immediately after a tributary flood. As the sediment becomes depleted at individual locations through ongoing downstream transport and winnowing of the channel bed, the sand on the bed and in suspension coarsens (Topping and others, 2000b). This fining of the sediment immediately following tributary floods and subsequent coarsening is not likely restricted to sand-size sediment, but also likely occurs in silt-and-clay-sized sediment. For a given sediment concentration, larger particles have a smaller surface area than an equal concentration of smaller particles, and the scattering of light is mainly a function of the surface area of the particles (Gilvear and Petts, 1985). Because of the supply-driven grain-size changes that occur in the suspended sediment in the Colorado River (Topping and others, 2000b), turbidity will likely increase rapidly as the clay-sized sediment from a flood on an upstream tributary arrives at a monitoring station. Then, as the suspended sediment at the monitoring station becomes dominated by progressively coarser size classes of sediment (silt, then ultimately sand), turbidity may decrease even if suspended-sediment concentration continues to increase or remains constant (Gippel, 1989). The dependence of turbidity on grain size in the study area is highlighted in figure 4, which shows that samples dominated by clay-sized sediment (circled in blue) have significantly higher turbidity relative to suspended-sediment concentration than samples dominated by silt-and-sand-sized sediment (circled in red). When the USGS guideline is not met, the USGS recommends developing a multiple linear regression (MLR) model using turbidity, SSC, and discharge. In the study area, the MLR showed no improvement over the SLR because of the poor correlation between discharge and suspended-sediment concentration (fig. 3).

Table 3. Summary of regression analysis of sediment concentration (total sediment and silt and clay) as a function of turbidity at the four monitoring stations below the CRLF station (see table 1; fig. 1).

[Based on the Breusch-Pagan tests, considering the study area as a whole, the \log_{10} -transformed model does a better job at reducing heteroscedasticity than the linear model for both total sediment and silt and clay (higher p-value). From a visual analysis of the residual plots, it was determined that, over the study area, using a linear model did not reduce curvature of the plots for either total sediment or silt and clay concentration]

Station identifier	Linear model	\log_{10} -transformed	Total sediment	Silt and clay	Breusch-Pagan test, p-value	Curvature of plot
CR030	X		X		7.6E-38	Moderate
CR030		X	X		0.082	Moderate
CR061	X		X		1.55E-62	Moderate
CR061		X	X		1.0E-7	No
CR087	X		X		7.8E-8	Moderate
CR087		X	X		0.21	No
CR225	X		X		7.8E-10	Moderate
CR225		X	X		0.74	Moderate
CR030	X			X	0.00056	No
CR030		X		X	0.001	Moderate
CR061	X			X	5.8E-14	Moderate
CR061		X		X	0.42	Moderate
CR087	X			X	5.5E-8	Moderate
CR087		X		X	0.71	No
CR225	X			X	1.9E-10	Moderate
CR225		X		X	0.50	No

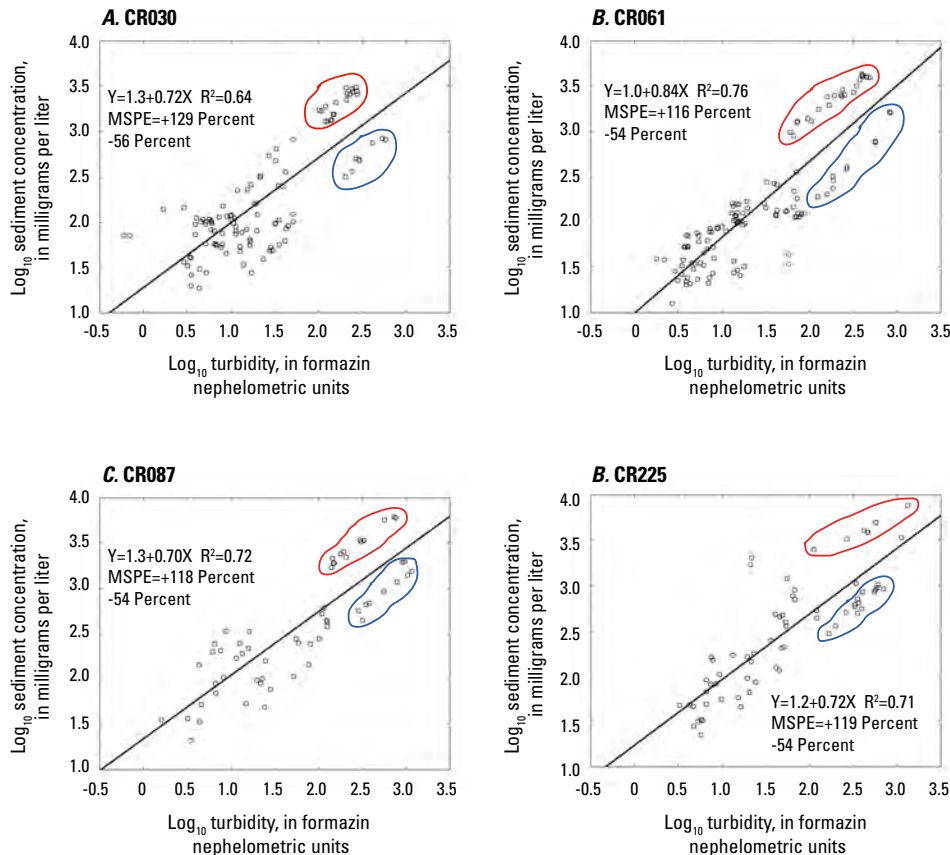


Figure 4. Graphs showing relations between \log_{10} of turbidity and \log_{10} of total suspended-sediment concentration at the four monitoring stations downstream from Lees Ferry: (A) at Colorado River near river mile 30 (CR030); (B) at Colorado River near river mile 61 (CR061); (C) at Colorado River near Grand Canyon, AZ, gaging station (CR087); (D) at Colorado River above Diamond Creek near Peach Springs, AZ, gaging station (CR225). For each graph, the equation of the regression line and the coefficient of determination are given. Suspended-sediment concentrations depicted in these plots are velocity-weighted concentrations in the river cross sections at these study sites. Suspended sediment was collected using either the Equal-Width-Increment method or the Equal-Discharge-Increment method (Edwards and Glysson, 1999). Samples dominated by clay-sized sediment are circled in blue and samples dominated by silt-and-sand-sized sediment are circled in red. Model standard percentage errors (MSPE) are the root-mean-square error expressed as percentages (Rasmussen and others, 2009).

10 Extending the Turbidity Record—Using Continuous Instrument Data and Suspended-Sediment Samples

Perhaps the most significant reason for not using turbidity as a surrogate for suspended-sediment concentration in the study area is that the operational range of the turbidity probes does not capture the entire range of suspended-sediment concentration. The upper limit of the measurable turbidity on optical turbidity probes, or the maximum recording level, is reached when the concentration of particles exceeds a certain level, causing multiple scattering and absorption, which results in a rapid drop in the scattered light reaching the nephelometric detectors (Sadar, 1998). The maximum recording level of the turbidity probes (fig. 5) in this study ranged from approximately 1,000 to 2,300 FNU (rarely above 1,600 FNU); the maximum recording level changed slightly during calibration and the maximum recording level of each probe differed. The maximum recording level of the turbidity probes at the monitoring stations was reached an average of only 3 percent of the

time (table 4). However, these periods of turbidity at or greater than the maximum recording level represented times when the highest sediment loads were reached in the study area and thus likely represented a substantial percentage (that is, most) of the total load during the study period. In the study area, the highest suspended-sediment concentration measured when turbidity was still below the maximum recording level of the turbidity probe was approximately 7,500 mg/L. During the study period, suspended-sediment concentrations of approximately 20,000 mg/L were reached, and thus approximately 60 percent of the range in suspended-sediment concentration had unmeasurable turbidity (that is, at or above the maximum recording level of the turbidity probes). For this reason alone, turbidity measured in the study area was not an acceptable surrogate for estimating suspended-sediment concentrations (Blanchard and Schertz, 2009).

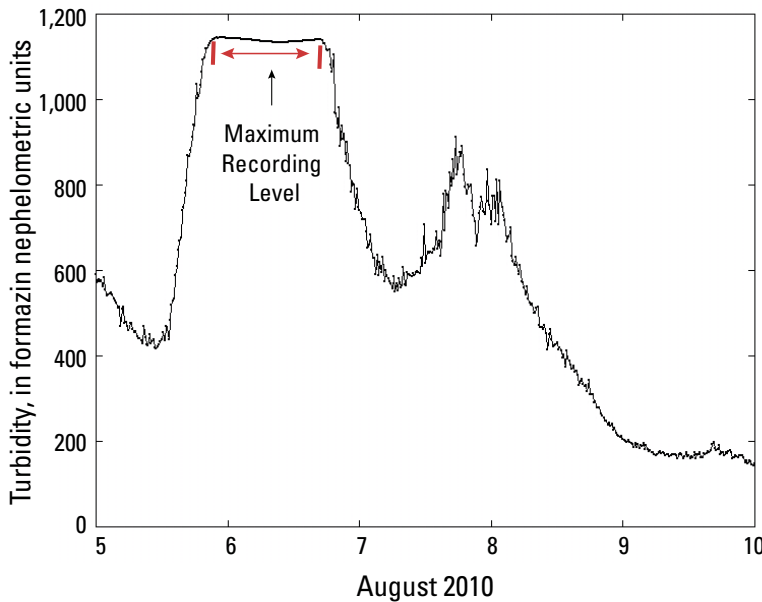


Figure 5. Time series of turbidity of the Colorado River at the CR225 monitoring station during 5–10 August 2010, showing data at the maximum recording level of the turbidity probe during part of that time. Turbidity when maximum recording level is reached is unknown, with actual turbidity equal to or greater than the maximum recording level.

Table 4. Summary of turbidity statistics over the periods of record for all monitoring stations.

[Percent of missing data represent the percentage of missing data over the station’s period of record (table 1)]

Station name	Station identifier	Percent of missing data	Percent of data that are above the maximum recording level of the turbidity probe
Colorado River at Lees Ferry, Arizona, USGS gaging station 09380000	CRLF	52	0
Colorado River near river mile 30	CR030	10	1
Colorado River near river mile 61	CR061	11	1
Colorado River near Grand Canyon, Arizona, USGS gaging station 09402500	CR087	4	6
Colorado River above Diamond Creek near Peach Springs, Arizona, USGS gaging station 09404200	CR225	6	7

Acoustic Attenuation and Backscatter

The side-looking ADPs deployed at the four monitoring stations in the study area downstream from the CRLF station were used to compute suspended-silt-and-clay concentrations, suspended-sand concentrations, and suspended-sand median grain size using the methods of Topping and others (2004, 2006, 2007). There are 1- and 2-MHz ADPs deployed at the four stations and an additional 600-kHz ADP at the CR087 monitoring station. The acoustic suspended-sediment measurements made by these instruments are initially calibrated by EDI or EWI measurements and then verified by subsequent EDI or EWI measurements. The ADPs provide several advantages over the use of turbidity as a surrogate for suspended-sediment concentration. The measurement range of the acoustic instruments covers the entire range of the suspended-sediment concentrations observed in the study area. Measurements from the acoustic instruments allow for discriminating finer sediment (principally silt-and-clay) from sand-sized suspended sediment. At a given frequency of sound, suspended sediment can be segregated into two acoustic size classes: (1) a finer acoustic size class in which increasing concentration (or decreasing grain size at a constant concentration) results mainly in increased attenuation of sound due to viscous losses (Urlick, 1948; Flammer, 1962; Lohrmann, 2001; Gartner, 2004; Topping and others, 2004, 2006, 2007; Wall and others, 2006; Wright and others, 2010) and (2) a coarser acoustic size class in which increasing concentration (or increasing grain size at a constant concentration) results mainly in increased backscatter of sound (Thorne and Campbell, 1992; Thorne and others, 1993; Thorne and Hanes, 2002; Lohrmann, 2001; Gartner, 2004; Topping and others, 2004, 2006, 2007; Wall and others, 2006; Wright and others, 2010). Silt and clay therefore typically dominate acoustic attenuation, whereas sand typically dominates acoustic backscatter (Topping and others, 2007; Wright and others, 2010). The major exceptions to this rule are as follows: at high sand concentrations ($>1,000$ mg/L), sand also contributes to acoustic attenuation, and at high ratios of silt and clay to sand concentration, silt and clay also contribute to acoustic backscatter (Thorne and Campbell, 1992; Topping and others, 2007). The measure of acoustic attenuation is the acoustic sediment attenuation coefficient, which is linearly related to suspended-silt-and-clay concentration when the following conditions are met: constant acoustic frequency, constant grain size and silt and clay mineral content, and sand concentrations lower than about 1,000 mg/L (Urlick, 1948; Flammer, 1962; Topping and others, 2007).

In this study, and as described by Topping and others (2007), the acoustic sediment attenuation coefficient was calculated for each ADP by (1) removing the two-way transmission losses associated with beam spreading and water absorption and (2) using linear regression to solve for the value of the acoustic sediment attenuation coefficient. The concentration of sand-sized sediment in discrete size classes was calculated from sediment-attenuation-corrected acoustic backscatter using a form of the sonar equation (Urlick, 1975; Topping and

others, 2007). In this approach, backscatter at higher frequencies is more sensitive to changes in the concentration of finer size classes of sand, thus allowing for the calculation of sand median grain sizes when multiple frequencies of ADPs are present. Similar to turbidity measurements, acoustic measurements of both the attenuation and backscatter caused by sediment are dependent on grain size. For example, the acoustic sediment attenuation coefficient is an order of magnitude larger for clay-sized particles than for the same concentration of coarse-silt-sized particles (Flammer, 1962). Thus, large changes in the grain-size distribution of silt and clay will result in similar large differences in both turbidity and in acoustic attenuation. For example, a given concentration of clay will result in much greater turbidity and acoustic attenuation than the identical concentration of silt.

Comparing Different Types of Data

Acoustic Attenuation and Turbidity

Acoustic attenuation can be divided into absorption and scattering components. The relative importance of these two components is determined by the grain-size distribution of the suspended sediment and the frequency of the acoustic instrument (Dukhin and Goetz, 2002). The dominant mechanism of acoustic attenuation in the Colorado River in Grand Canyon, based on the grain-size distribution and frequency of ADPs, is absorption through viscous losses. Acoustic attenuation from viscous losses, which is caused by shear friction at the particle fluid boundary, is represented on the left side of figure 6, which shows the theoretical relation between the acoustic sediment attenuation coefficient for a given suspended-sediment concentration and grain size at a frequency of 1 MHz (Wright and others, 2010). As frequency increases, this relation shifts up and to the left. For example, the same plot for a frequency of 2 MHz would be slightly up and to the left of the 1-MHz plot in figure 6 (see fig. 2B in Topping and others, 2007). As suspended-sediment grain size increases above about 2 microns, the acoustic sediment attenuation coefficient decreases for a given suspended-sediment concentration when measured with a 1-MHz ADP.

The acoustic sediment attenuation coefficient, although affected by grain size (fig. 6), is strongly and linearly correlated with the concentration of silt and clay in the study area (Topping and others, 2007). As log-transformed turbidity is also strongly and linearly correlated with log-transformed silt and clay concentration (fig. 7), it follows that log-transformed turbidity and the log-transformed acoustic sediment attenuation coefficient should also be linearly related. When lower values of log-transformed acoustic sediment attenuation coefficient (\log_{10} of acoustic sediment attenuation coefficient <-0.65) and turbidity (\log_{10} of turbidity <1.6) are not included in the linear model, log transformation of the data reduces

heteroscedasticity and curvature, and the goodness of fit is better than the nontransformed linear model (fig 8). Excluding the lower turbidity (<40 FNU) and acoustic-sediment-attenuation-coefficient data from the model is warranted, because (1) the higher uncertainty at lower turbidity and acoustic-sediment-attenuation-coefficient values is magnified when log transforming the data and (2) the model is intended to be used only to estimate high turbidity above the maximum recording level of the turbidity instruments (that is, through extrapolation).

The correlation between log-transformed turbidity and the log-transformed acoustic sediment attenuation coefficient is, in general, better than the correlation between log-transformed turbidity and the log-transformed silt and clay concentration determined from the EWI, EDI, and pump measurements at the monitoring stations. One possible explanation for this is that both log-transformed turbidity and the log-transformed acoustic sediment attenuation coefficient respond similarly to variations in grain size distributions. By

this explanation, there is a particular grain size (x), somewhere in the clay grain-size range, that results in the highest turbidity or acoustic attenuation (from viscous losses) for a given sediment concentration. The value of this grain size (x), which will be different for turbidity and acoustic attenuation, will vary depending on the physical parameters of the sediment as well as the design components of the instruments that measure turbidity and acoustic attenuation. For grain sizes larger than this threshold value, log-transformed turbidity and the log-transformed acoustic sediment attenuation coefficient both decrease per unit log-transformed concentration. Thus, assuming that grain size (x) is similar for turbidity and acoustic attenuation, for a given concentration of sediment, as grain size progressively increases into the coarser clay, silt, and fine-sand size classes, both log-transformed turbidity and the log-transformed acoustic sediment attenuation coefficient decrease.

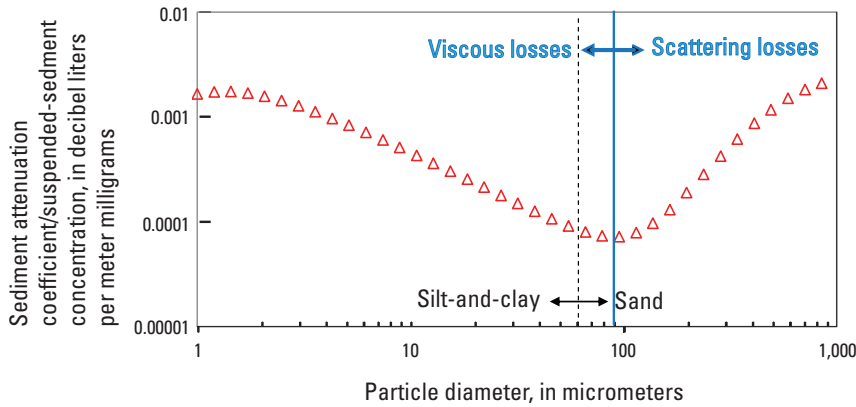


Figure 6. Graph showing theoretical variation in the 1-MHz acoustic sediment attenuation coefficient, relative to suspended-sediment concentration (y-axis), compared against changing particle size (x-axis). This figure is modified from Wright and others (2010) and is based on theoretical relations developed and tested by Urlick (1948), Flammer (1962), and Thorne and Hanes (2002).

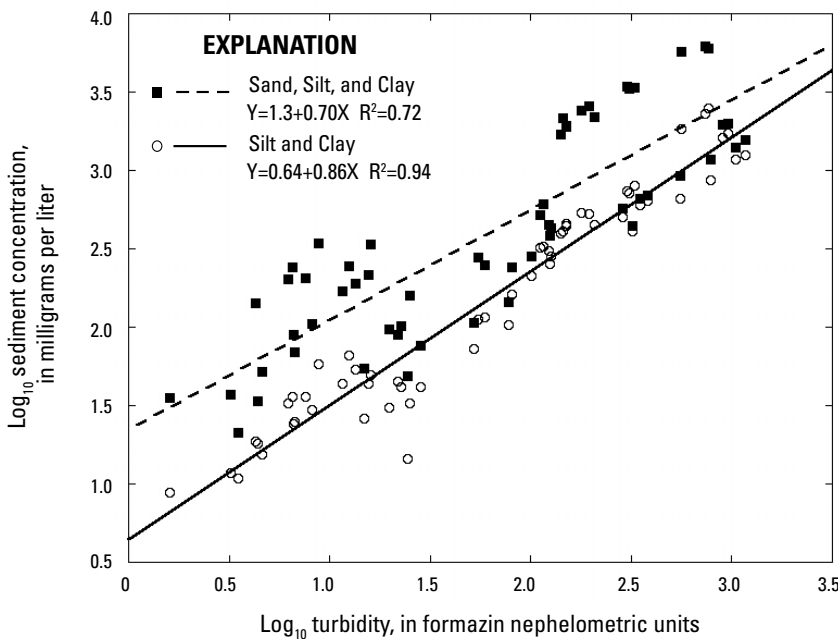


Figure 7. Graph showing relation between \log_{10} of turbidity and \log_{10} of suspended-sediment concentration of total sediment (sand, silt, and clay) and of silt and clay alone at the CR087 monitoring station. The equation of the regression line and the coefficient of determination are given for each. Suspended-sediment concentrations depicted in this plot are velocity-weighted concentrations in the river cross section at this study site. Suspended sediment was collected using the Equal-Discharge-Increment method (Edwards and Glysson, 1999). For each total suspended-sediment concentration (sand, silt, and clay) shown in the figure, there is a corresponding silt-and-clay concentration calculated after mechanically separating (by wet sieving) the silt and clay from the sand in the laboratory (Poppe and Polloni, 2000). These two concentrations (total sediment and silt and clay) from the same collected sample have the same turbidity value in the figure (the turbidity measured during the time of sample collection).

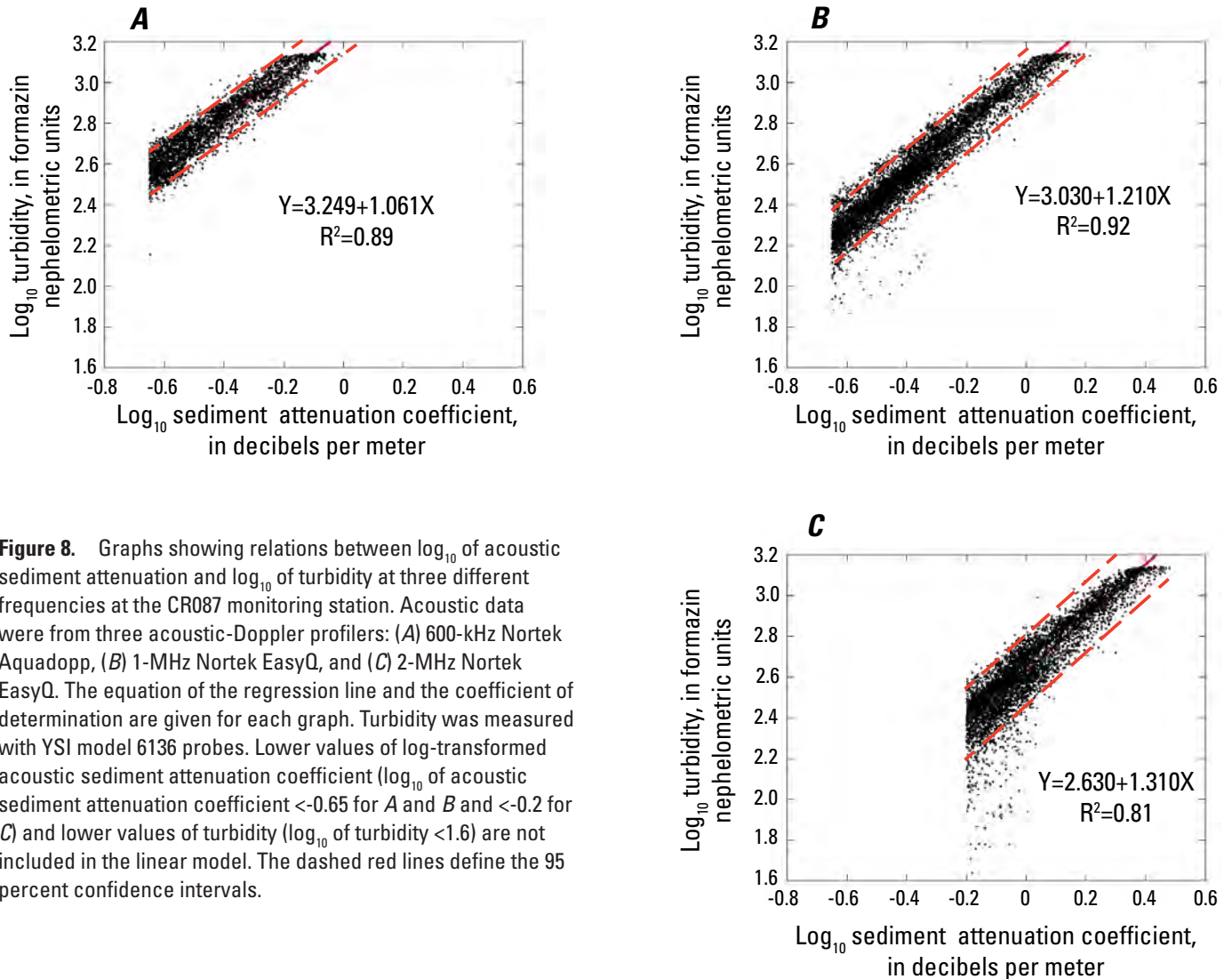


Figure 8. Graphs showing relations between log₁₀ of acoustic sediment attenuation and log₁₀ of turbidity at three different frequencies at the CR087 monitoring station. Acoustic data were from three acoustic-Doppler profilers: (A) 600-kHz Nortek Aquadopp, (B) 1-MHz Nortek EasyQ, and (C) 2-MHz Nortek EasyQ. The equation of the regression line and the coefficient of determination are given for each graph. Turbidity was measured with YSI model 6136 probes. Lower values of log-transformed acoustic sediment attenuation coefficient (log₁₀ of acoustic sediment attenuation coefficient <-0.65 for A and B and <-0.2 for C) and lower values of turbidity (log₁₀ of turbidity <1.6) are not included in the linear model. The dashed red lines define the 95 percent confidence intervals.

Extending the Turbidity Record

Extending the turbidity record by estimating the unmeasurable turbidity (above the maximum recording level of the turbidity instruments) allows biologists to estimate the upper limit of the suspended sediment's influence on light availability as it relates to (1) fish behavior and (2) other parameters, such as gross primary production. At each monitoring station, turbidity above the maximum recording level of the optical turbidity instrument was estimated from the simple linear regression relating log-transformed turbidity to the log-transformed acoustic sediment attenuation coefficient from the 1-MHz ADP (figs. 8 and 9). The acoustic sediment attenuation coefficient from the 1-MHz ADP was chosen, because it correlated somewhat better with turbidity and had a longer and more continuous record than the acoustic sediment attenuation coefficient from the 2-MHz ADP (or the 600-kHz ADP at the CR087 monitoring station). A single linear regression model for estimating turbidity above the maximum recording level of the instruments was developed for the four stations

downstream from the CRLF station by pooling the data from all four stations. This model is

$$y = 2.985 + 1.114x \quad (4)$$

where y is log₁₀ of turbidity and x is log₁₀ of 1-MHz acoustic sediment attenuation coefficient. The coefficient of determination (R^2) of the model is 0.82, and the residual standard error is 0.114. The decision to pool data from the four stations to generate a single regression was based primarily on the similarity (within 10 percent) of the linear regressions of the 1-MHz acoustic sediment attenuation coefficient and silt and clay concentration among the stations. In these regressions, the measured 1-MHz acoustic sediment attenuation coefficient covers the entire range of silt and clay concentration in the study area. Thus, considering the similarity among these regressions, and the fact that turbidity in the study area is primarily caused by silt and clay concentration, particularly at higher turbidity levels (see figs. 7 and 23 [presented later

in this report]), using a single regression was determined to be the best option to estimate turbidity above the maximum recording level of the instruments in the study area.

Turbidity at the CRLF station, located upstream from the first major tributary in the study area, was always below the maximum recording level of the optical turbidity instruments (fig. 9). At all stations downstream from the Paria River, there are estimated turbidity values (above the maximum recording level of the optical turbidity instruments) for each year of the study (figs. 9 and 10). As expected, turbidity is generally higher during the summer and fall thunderstorm season, when the tributaries are more frequently flooding and supplying sediment to the Colorado River. A box-and-whisker plot of the measured and estimated turbidity record at all monitoring stations in the study area shows that the stations are grouped according to their position relative to the two major tributaries in the study area (fig. 11). The two stations located between the Paria River and Little Colorado River (CR030 and CR061) have similar turbidity, as do the two stations downstream from the Little Colorado River (CR087 and CR225).

A comparison was made between turbidity levels in Grand Canyon before and after the building of Glen Canyon Dam. Systematic turbidity measurements were not made in the study area before dam construction; pre-dam turbidity estimates are based on the daily suspended-sediment record and the relation between turbidity and suspended-silt-and-clay concentration described above. Post-dam turbidity in figure 12 is from the turbidity record established during this study, with turbidity above the recording level of the optical

instruments estimated from concurrent 1-MHz acoustic data at the same location (that is, the same data as in figure 9). From these estimates, average pre-dam turbidity was higher than post-dam turbidity by an average of a factor of approximately 2,000 at the CRLF station and approximately 20 at the CR087 station. The pre- and post-dam turbidity differences between these two stations are not unexpected, because suspended sediment passing the Lees Ferry station has been almost completely eliminated with the construction of Glen Canyon Dam, whereas the CR087 station still receives sediment from major tributaries of the Colorado River downstream from the dam. A turbidity-duration comparison of pre- and post-dam turbidity in the study area is also presented in figure 13. Figure 13B shows a 5-year post-dam period of common record at all five monitoring stations. At the farthest upstream station, CRLF, the water was clear most of the time. As is also shown in figure 11, turbidity increases in a stepwise fashion in the downstream direction, with increases mainly caused by the Paria and Little Colorado Rivers. The other tributaries have very little influence on turbidity in the Colorado River. As a result of the influence of the Paria River, turbidity increases by a factor of approximately 8 between the CRLF and CR030 stations and then increases only slightly between the CR030 and CR061 stations. As a result of the influence of the Little Colorado River, turbidity increases by a factor of approximately 4 between the CR061 and CR087 stations and then increases only slightly between the CR087 and CR225 stations. Compared to the pre-dam river, turbidity is generally very low in the post-dam river throughout all of Grand Canyon.

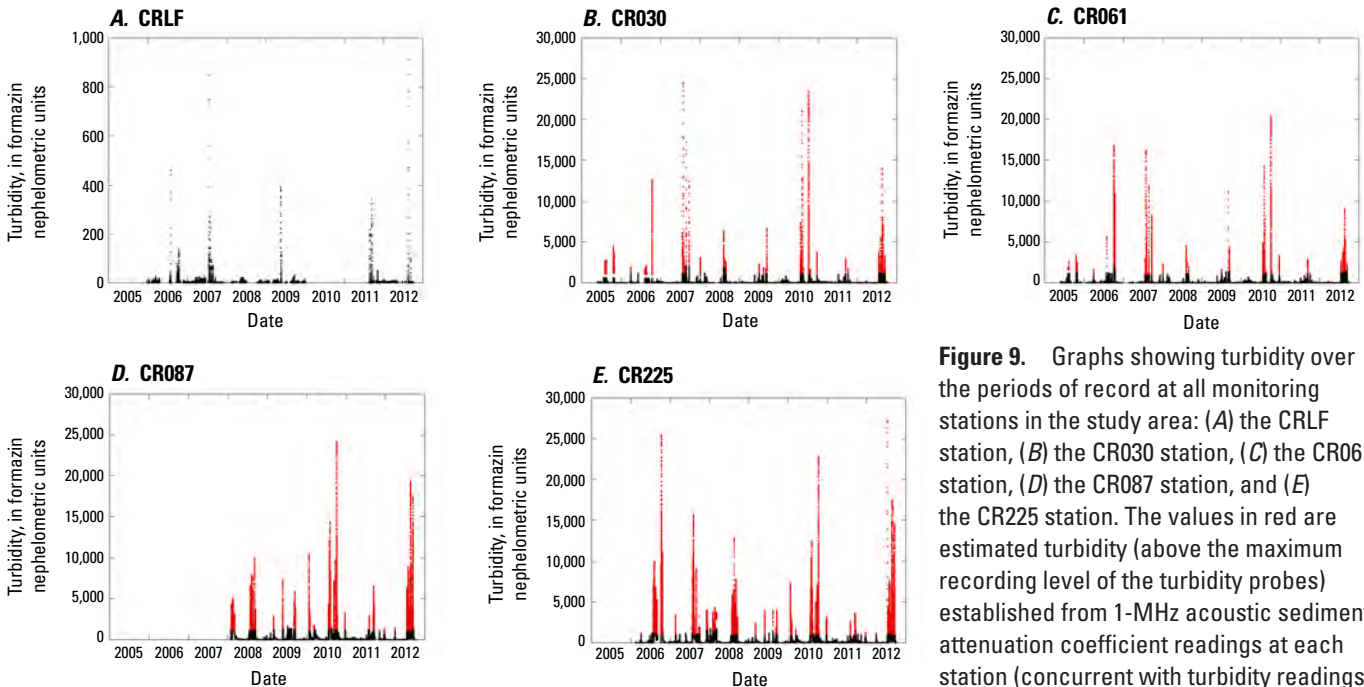


Figure 9. Graphs showing turbidity over the periods of record at all monitoring stations in the study area: (A) the CRLF station, (B) the CR030 station, (C) the CR061 station, (D) the CR087 station, and (E) the CR225 station. The values in red are estimated turbidity (above the maximum recording level of the turbidity probes) established from 1-MHz acoustic sediment attenuation coefficient readings at each station (concurrent with turbidity readings)

and the single linear regression model (for all four stations below CRLF) of \log_{10} of the acoustic sediment attenuation coefficient from 1-MHz acoustic-Doppler profiler measurements and \log_{10} of concurrent turbidity measurements (see equation 4 in text). The reported turbidity estimates (shown in red) represent the mean of the regression model. Applying a 95-percent confidence interval, there is an approximately 2.8-fold range in estimated turbidity for a given acoustic sediment attenuation coefficient (see fig. 10). Note that the y-axis scale (turbidity) for the CRLF station plot is different from those on the other plots.

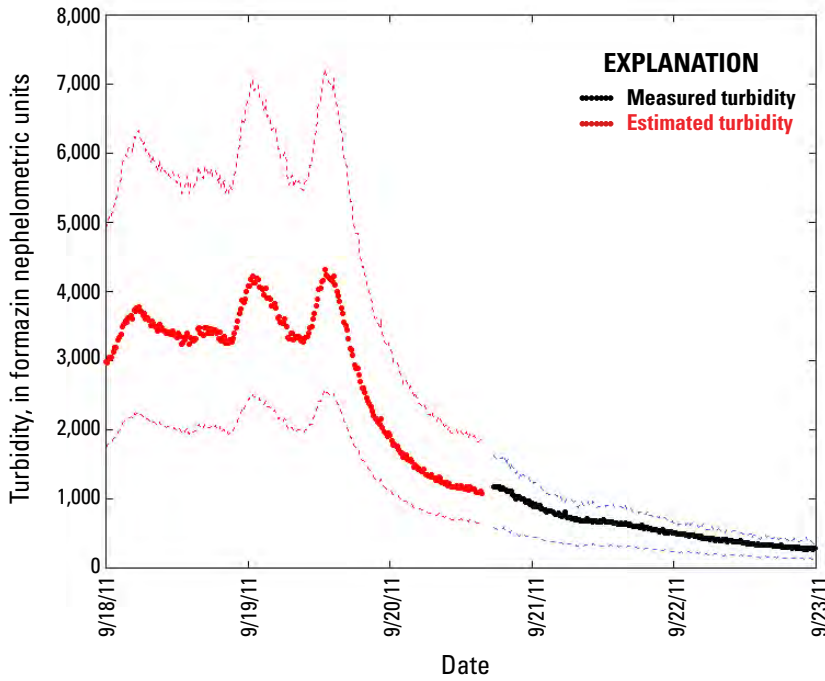


Figure 10. Graph of measured (shown in black) and estimated (shown in red) turbidity at the CR087 monitoring station from September 18 to 23, 2011. Estimated turbidity (above the maximum recording level of the turbidity probes) was established from 1-MHz-acoustic-sediment-attenuation-coefficient readings at the CR087 station and the regression model of \log_{10} of the 1-MHz acoustic sediment attenuation coefficient and \log_{10} of concurrent turbidity measurements (see equation 4 in text). The red and blue dashed lines show the 95-percent confidence interval around the mean, with the blue lines established from 1-MHz-acoustic-sediment-attenuation-coefficient readings taken concurrently with the measured turbidity (shown in black). Note that the measured turbidity values are within the 95-percent confidence interval of the regression model, and the confidence interval is asymmetric around the mean (estimated turbidity), because the interval was computed on log-transformed data.

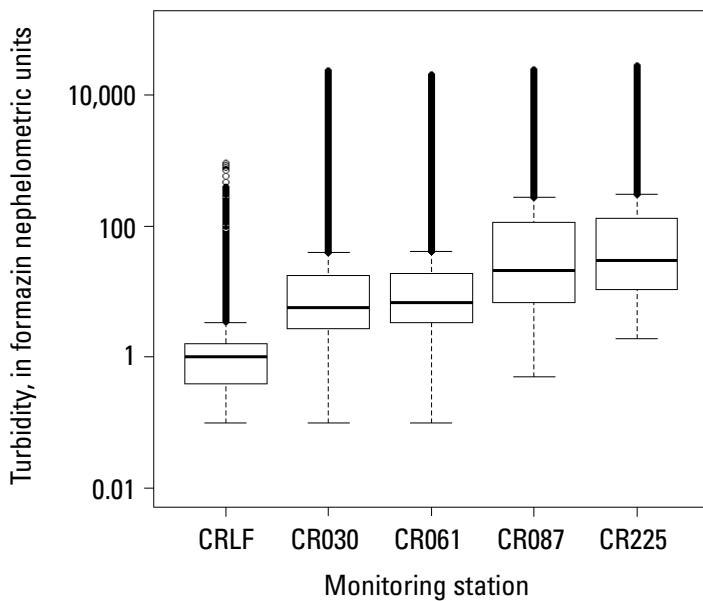


Figure 11. Box and whisker plots of turbidity during the period of record common to all five monitoring stations, January 29, 2008, through October 1, 2012. The line in the box shows the median. The boxes extend to the upper and lower quartiles. The whiskers extend to the 10th and 90th percentiles, and the points above the upper whisker represent all points greater than the 90th percentile. See table 1 for an explanation of the monitoring station identifiers. Turbidity is estimated when above the maximum recording level of the probes using the relation between \log_{10} of the acoustic sediment attenuation coefficient from 1-MHz acoustic-Doppler profiler measurements and \log_{10} of concurrent turbidity measurements (see equation 4 in text).

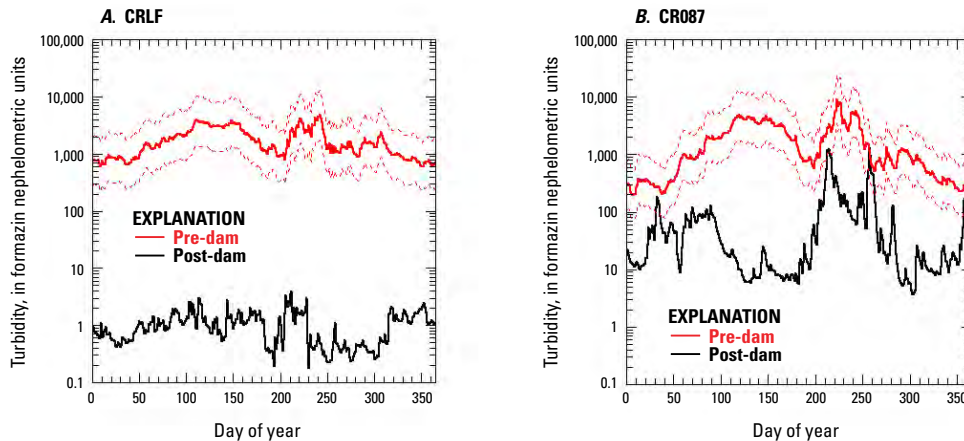


Figure 12. Graphs showing geometric daily mean turbidity at the (A) CRLF and (B) CR087 monitoring stations through the course of the year. Values in red depict the geometric daily mean turbidity estimated on the basis of the pre-dam USGS daily suspended-sediment record and the CR087 relation between \log_{10} of suspended-silt-and-clay concentration and \log_{10} of turbidity established in this study (used for both the CRLF and CR087 stations, because pre-dam sediment loads were mostly composed of silt and clay). The period of pre-dam daily sediment record (using modern isokinetic samplers) at the CRLF station is October 1, 1947, through February 10, 1959, and at the CR087 station it is June 1, 1944, through July 31, 1958. Closure of the coffer dam at the Glen Canyon dam site on February 11, 1959, began the trend toward unnaturally clearer water. Values in black depict the geometric daily mean turbidity after the construction of Glen Canyon Dam, over the periods of record of this study (table 1, fig. 9). Geometric means were used (as opposed to arithmetic means) as the measure of the central tendency of the distributions of the average turbidity on any given day of the year because these distributions are highly right skewed. The red dashed lines show the 95-percent confidence interval for pre-dam values established from the post-dam linear model of \log_{10} of suspended-silt-and-clay concentration and \log_{10} of turbidity at the CR087 station. While considering additional uncertainty from using a regression developed post-dam for pre-dam conditions, pre-dam turbidity at the CRLF and CR087 stations was significantly higher than post-dam turbidity at those stations, except for perhaps during approximately 2 to 15 days out of the year at the CR087 station when pre- and post-dam turbidity levels were comparable.

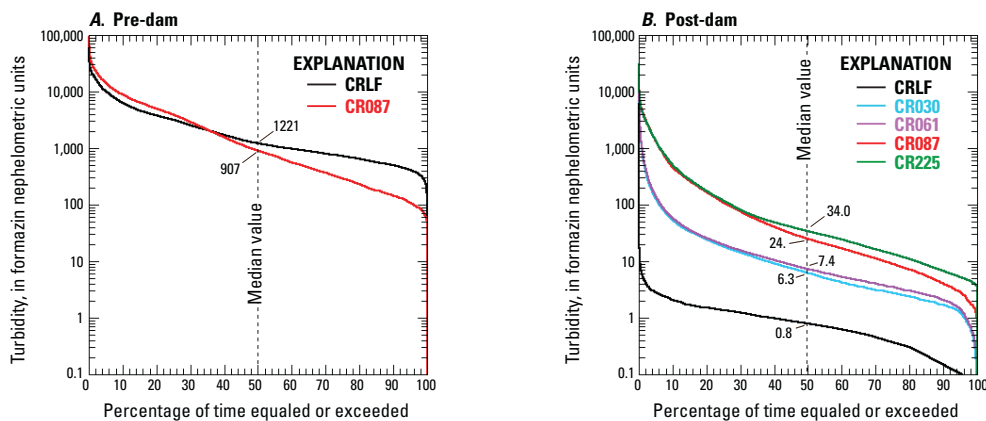


Figure 13. Pre- and post-dam turbidity duration plots. A, Estimated turbidity at the CRLF and CR087 monitoring stations plotted as a function of the time equaled or exceeded during the pre-dam period of continuous (that is, no substantial data gaps) daily sediment data common to both monitoring stations, October 1, 1947, through June 1, 1956. Pre-dam turbidity was likely higher at the CRLF station than at the CR087 station ~64 percent of the time because more of the sediment load occurred during fewer days of the year at the CR087 station than at the CRLF station. Pre-dam turbidity is estimated to have exceeded ~1,221 formazin nephelometric units (FNU) half of the time at the CRLF station and ~907 FNU half of the time at the CR087 station. Turbidity estimates are based on the pre-dam USGS daily suspended-sediment record and the CR087 relation between suspended-silt-and-clay concentration and turbidity established in this study (used for both the CRLF and CR087 stations, because pre-dam sediment loads were mostly composed of silt and clay). B, Measured turbidity and estimated turbidity (when above the maximum recording level of the turbidity probes) based on the relation between \log_{10} of the acoustic sediment attenuation coefficient and \log_{10} of concurrent turbidity measurements (see equation 4 in text), at the CRLF, CR030, CR061, CR087, and the CR225 monitoring stations during the post-dam period of continuous data common to all five monitoring stations, January 2008 through fall 2012. During this nearly 5-year post-dam period, turbidity exceeded ~0.8 FNU half of the time at the CRLF station, ~6.3 FNU half of the time at the CR030 station, ~7.4 FNU half of the time at the CR061 station, ~24.9 FNU half of the time at the CR087 station, and ~34.0 FNU half of the time at the CR225 station.

Laser Diffraction and Transmission

Sequoia Scientific LISST-100C laser-diffraction instruments with 1-cm path lengths were deployed in the Colorado River near the bank at the CR061 and CR087 stations. The point data collected using these instruments were calibrated using EDI and EWI measurements to measure velocity-weighted concentrations of suspended sand in multiple size classes in the cross sections at these stations (Topping and others, 2006). In addition to the EDI and EWI measurements, pump measurements were also used to provide additional information in the development of the silt and clay parts of these calibration relations.

The LISST-100C instrument, using a combination of laser transmittance and diffraction, is designed to measure the volumetric sediment concentration of 32 size classes of particles between approximately 2.5 and 500 microns (Agrawal and others, 2008). The LISST instrument operates under the principle that different grain sizes diffract light at different angles, with the larger grains diffracting light at smaller angles. A series of ring detectors is located in front of the laser with each ring sampling a different size class. Thus, the LISST instrument may offer an advantage over turbidity and acoustic instruments in that the LISST instrument, in theory, outputs total sediment concentration data that are not grain-size dependent; the total concentration is calculated as the sum of the concentration of the size classes. In this study, the LISST-100 data were processed with the standard assumption of spherical particles using Mie theory (Agrawal and Pottsmith, 2000). A newer approach that imposes an assumed more natural particle shape (Agrawal and others, 2008) was not available when most of the LISST-100 data in this study were collected and processed. Use of the newer theory would not have affected the results in this study because: (1) use of the standard or new theory does not affect measured beam transmittance, and (2) the required calibration of the point LISST-100 data to provide velocity-weighted measurements of suspended-sediment concentrations in the river cross sections would result in identical calibrated concentrations using either theory.

Figure 14 shows the relation between turbidity and silt and clay concentration as measured by the LISST-100C instruments at the CR061 and CR087 monitoring stations. Although the correlation between turbidity and LISST-measured silt and clay concentration is reasonably good, the linear regression at both stations is unsatisfactory as a result of heteroscedasticity (the variance in LISST-measured silt and clay concentration increases significantly with increasing values of turbidity). Although logarithmic transformation of both the independent and dependent variables in figure 14 would improve the correlation between turbidity and LISST-measured silt and clay concentration, the improved goodness of fit resulting from this logarithmic transformation is somewhat misleading, because both turbidity and LISST measurements of silt and clay concentration are similarly biased by grain-size change within the silt and clay grain-size range (fig. 15). When the finest fraction of the suspended sediment load is dominated by clay-sized

particles (as indicated by the LISST-100 measurements on individual rings and also the grain-size distributions presented later in this report in figure 21), both the turbidity probe and the LISST-100 tend to “overmeasure” silt and clay concentration (with estimated or predicted concentration higher than actual concentration, data circled in blue in figures 15A–D). As shown in figures 15A, B (data circled in red), when the fine fraction is dominated by silt-sized particles, the LISST-100C provides relatively accurate measurements of silt and clay concentration compared to the sampled concentration of silt and clay. However, when the silt and clay is dominated by clay-sized particles (data circled in blue), the LISST-100C measurements of silt and clay concentration are too high by about a factor of 2 to 3. Similarly, the effective relation between silt and clay concentration and turbidity “shifts upward” by about a factor of 2 to 3 when the dominant grain size of the silt and clay shifts from silt to clay (figures 15C, D). Thus, measurements of suspended-silt-and-clay concentration made using a LISST-100C laser diffraction instrument are no more accurate than those made using an optical turbidity probe. However, because the LISST-100C records information on the grain-size distribution on 32 rings, LISST measurements of silt and clay concentration could perhaps be made more accurate than turbidity measurements of silt and clay concentration by developing two calibration relations between LISST-measured and “true” silt and clay concentration—one for silt and one for clay.

The LISST instrument is also equipped with a transmissometer that measures a narrow collimated beam of light (670-nm wavelength) transmitted in a straight line through a 75-micron hole located at the center of the ring detectors. Ideally, the transmissometer measures the remaining quantity of light (the light source of the LISST-100C) that is not absorbed or scattered in water. This assumes that the transmissometer has a very small angle of view and is not measuring appreciable forward scattering of light; the LISST instrument satisfies the criterion of less than 1 degree for the half angle of the cone of detected light (Agrawal and others, 2008; Agrawal and Pottsmith, 2000; Davies-Colley and others, 1993). The beam transmittance value measured by a transmissometer can be converted into a beam attenuation coefficient (Davies-Colley and others, 1993):

$$T_c = \Phi_r / \Phi_0 \quad (5)$$

$$c = \ln(1/T_c) / r, \quad (6)$$

where T_c is the beam transmittance, Φ_r is the radiant power (light flux) of the transmitted beam after traveling distance r (the path length) through the water sample, Φ_0 is the light flux of the transmitted beam through pure water, and c is the beam attenuation coefficient. Turbidity is a relative scattering measurement that is instrument specific and does not relate simply to visual clarity (Davies-Colley and others, 1993). The beam attenuation coefficient, however, is an inherent optical

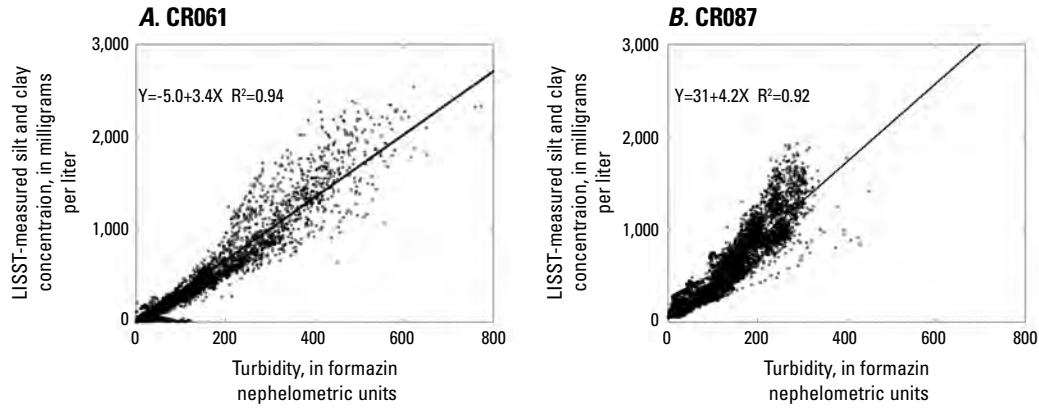


Figure 14. Graphs showing relations between turbidity and LISST-100C-measured silt and clay concentration at the (A) CR061 and (B) CR087 monitoring stations. The equation of the regression line and the coefficient of determination are given for each graph. The LISST-100C laser-diffraction instrument measures sediment concentration in microliters per liter; for consistency among the analyses in this report, LISST-measured concentrations have been converted to milligrams per liter assuming a quartz sediment density of 2.65 g/cm³.

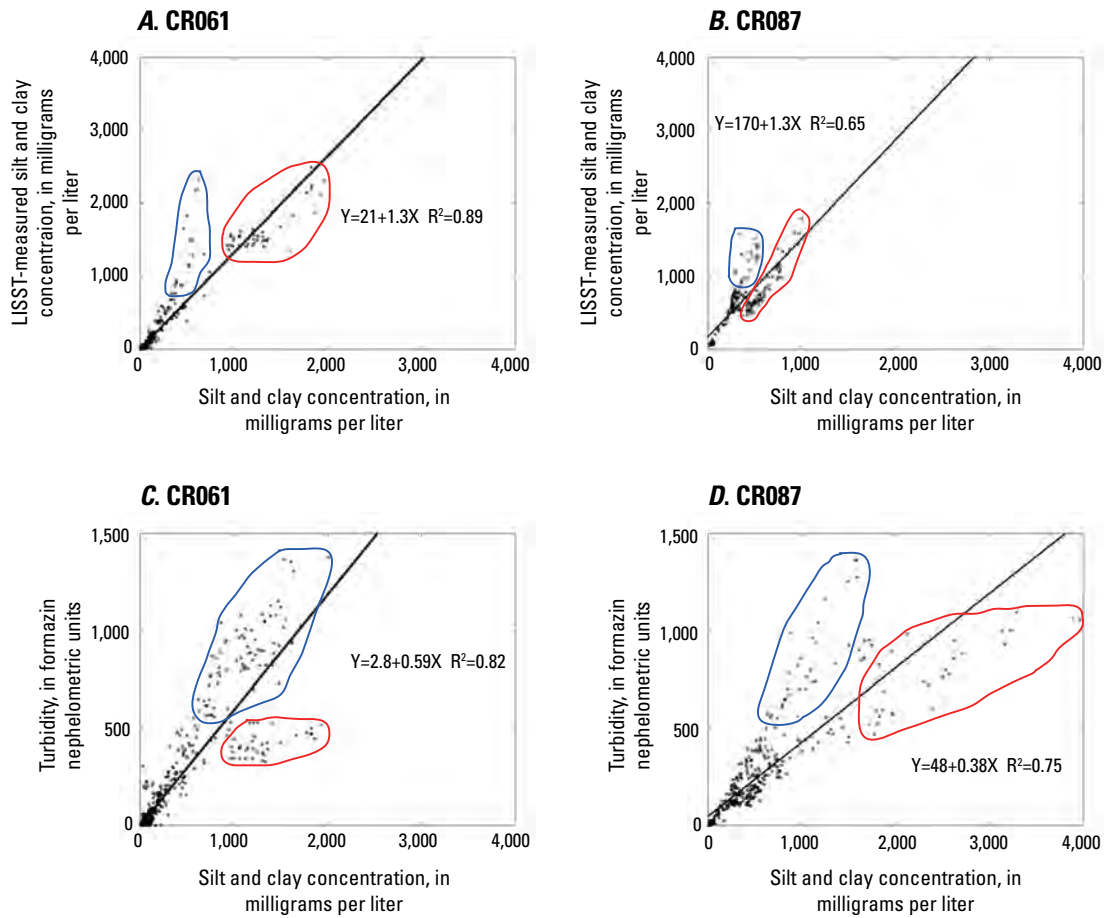


Figure 15. Graphs showing relations between sampled silt and clay concentration and LISST-100C-measured silt and clay concentration at the (A) CR061 and (B) CR087 monitoring stations compared with the relations between sampled silt and clay concentration and turbidity at the (C) CR061 and (D) CR087 monitoring stations. The equation of the regression line and the coefficient of determination are given for each graph. Sampled sediment concentrations depicted in these plots are from EWI, EDI, and cross-section-calibrated pump measurements made during June 20, 2005, through February 23, 2010, for A and C and during January 30, 2008, through February 25, 2010, for B and D. The LISST-100C laser-diffraction instrument measures sediment concentration in microliters per liter, which for consistency of units with the sampled concentrations has been converted to milligrams per liter assuming a quartz sediment density of 2.65 g/cm³. The "upper horn" in these data clouds (circled in blue) is dominated by clay-sized sediment, whereas the "lower horn" (circled in red) is dominated by silt-sized sediment (mostly from the 2008 controlled-flood experiment).

property of water that correlates closely with the visual range of an object (Davies-Colley and others, 1993), potentially making it a more useful parameter for estimating reactive distances between predator and prey (Aksnes and Giske, 1993).

The relation between turbidity and beam transmittance (fig. 16) is better than the relation between turbidity and silt and clay concentration measured by the LISST (fig. 14), especially at the CR087 monitoring station, which has less variability at lower beam transmittance (higher turbidity) than at the CR061 monitoring station. Sequoia Scientific recognizes that at beam transmittance values less than approximately 0.3 ($10^{-0.5}$) multiple scattering increases as beam transmittance decreases, which biases the grain-size distribution (Agrawal and Pottsmith, 2000). Beam transmittance appears to have a larger useable range at the two monitoring stations than the range reported by Sequoia Scientific (beam transmittance >0.3). The variance of beam transmittance as a function of turbidity is fairly constant for beam transmittance greater than approximately 0.25 ($10^{-0.6}$) at the CR061 station and approximately 0.06 ($10^{-1.2}$) at the CR087 station (fig. 16). These beam transmittance ranges correspond to turbidity ranges of less than approximately 200 FNU and 300 FNU at the CR061 and CR087 stations, respectively (fig. 16).

Without some modification to how the LISST measures clay-sized sediment, measurements of silt and clay concentration made using a LISST and a turbidity probe are equally poor. Despite the problem that the LISST tends to “overmeasure” the concentration of clay-sized sediment, the LISST-100 instrument, unlike a turbidity probe, is useful for determining how sediment concentration varies with grain size within the grain-size range of the instrument (Agrawal and Pottsmith, 2000; Agrawal and others, 2008). The LISST instrument also provides transmissometry data from which the beam attenuation coefficient can be calculated, an optical parameter that is more usable than turbidity from the standpoint of water clarity (Davies-Colley and others, 1993). A drawback of the LISST instrument is that, unlike the turbidity probes, the LISST does not have a mechanical wiper, and without a field visit to clean the lens, biological fouling reduces the LISST instrument data to unusable within a few weeks to a month at the CR061 and CR087 monitoring stations. Also, owing to multiple scattering, the suspended-sediment-concentration measurement range of the LISST instruments is less than half the range of the turbidity instruments used in the study.

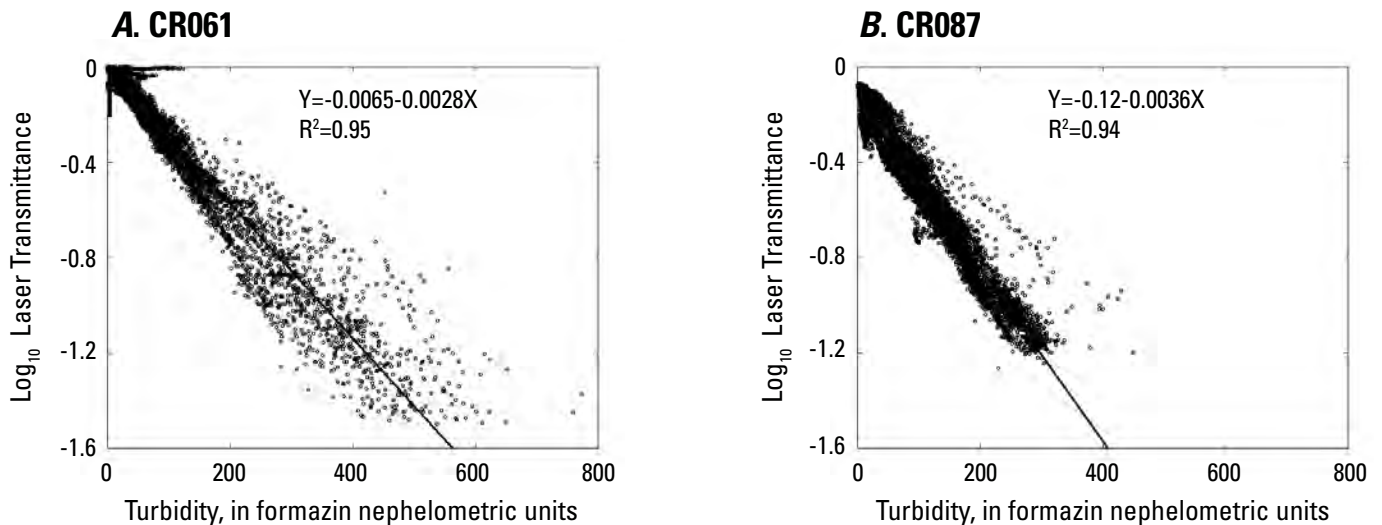


Figure 16. Graphs showing relations between turbidity and \log_{10} of laser transmittance measured using a LISST-100C laser-diffraction instrument at (A) the CR061 monitoring station from June 20, 2005, through June 26, 2010, and (B) the CR087 monitoring station from January 29, 2008, through June 15, 2010. The equation of the regression line and the coefficient of determination are given for each graph.

Physical Explanation for Apparent Data Outliers

Changes in the physical properties of the sediment in suspension will change the relations between suspended-sediment concentration and turbidity, between suspended-sediment concentration and the acoustic sediment attenuation coefficient, and between turbidity and the acoustic sediment attenuation coefficient. The physical properties that may change these relations are the mix of grain sizes, grain shapes, color, and clay-mineral content of the suspended sediment. With the exception of color, changes in any of these physical properties will affect all of these relations. Color does not affect sound, and therefore changes in color will have no influence on the relation between suspended-sediment concentration and the acoustic sediment attenuation coefficient. Because changes in the physical properties of the sediment in suspension will change the above relations, atypical sediment in suspension will result in apparent outliers to these relations. Large outliers are typically interpreted to represent mistakes or large measurement errors. However, the apparent outliers in the above relations are real, and therefore indicate the presence of suspended sediment derived from atypical and perhaps unique source areas. Thus, recognition that these apparent outliers represent atypical sediment properties may allow one to infer sediment provenance.

The relation between turbidity and the acoustic sediment attenuation coefficient may change as the physical properties of the suspended sediment change, because turbidity and the acoustic sediment attenuation coefficient respond differently to the various physical properties of the sediment. There are two groups of outliers on the plots relating turbidity and the

acoustic sediment attenuation coefficient: (1) data during the March 2008 controlled-flood experiment and (2) data from July 24, 2007 (fig. 17). The March 2008 outliers are present at all four monitoring stations downstream from the CRLF station, and the July 2007 outliers are present at the CR030 and CR061 stations (downstream from House Rock Wash). The outliers are evident in comparisons of optical turbidity measurements and acoustic-sediment-attenuation-coefficient measurements at 1- and 2-MHz frequencies at the CR030, CR061, CR087, and CR225 stations, and also at 600-kHz frequency at the CR087 station.

Data from both anomalous events also show up as apparent outliers when comparing data other than turbidity and the acoustic sediment attenuation coefficient. At the CR061 station, only one physical suspended-sediment sample was collected on July 24, 2007. The silt and clay concentration of that sample is associated with a concurrent 2-MHz acoustic sediment attenuation coefficient that is high relative to the regression (fig. 18). The 2008 controlled-flood-experiment data on this same plot fall on both sides of the regression line (fig. 18). Acoustic-sediment-attenuation-coefficient data from the 1-MHz ADP at the CR030 station show a similar trend (fig. 19). The 2008 controlled-flood-experiment samples collected at the CR061 station and analyzed for silt and clay concentration have low turbidity relative to the regression line (fig. 20). The single sample collected on July 24, 2007, at the CR061 station also has low turbidity relative to the regression line; however, the 2008 controlled-flood-experiment samples with comparable silt and clay concentrations have significantly lower turbidity and thus are larger apparent outliers (fig. 20).

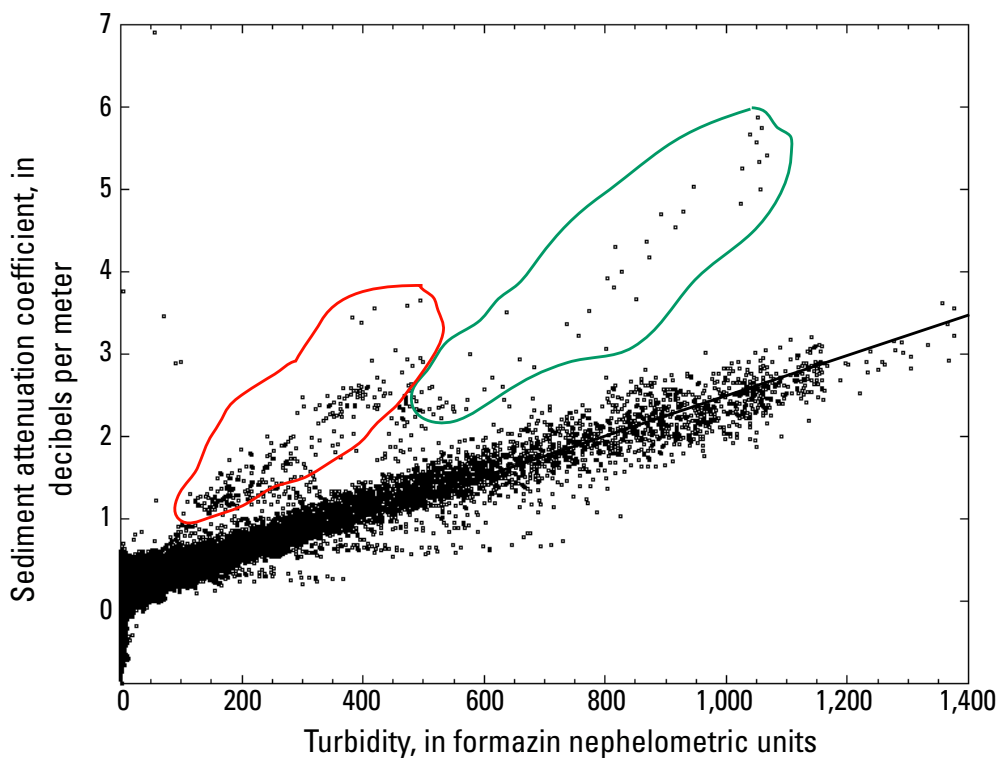


Figure 17. Graph showing relation between turbidity and the 2-MHz acoustic sediment attenuation coefficient calculated from data collected using a 2-MHz Nortek EasyQ acoustic-Doppler profiler at the CR061 monitoring station. The data circled in red are from the March 2008 controlled-flood experiment (Topping and others, 2010; Schmidt and Grams, 2011b), and the data circled in green are from July 24, 2007.

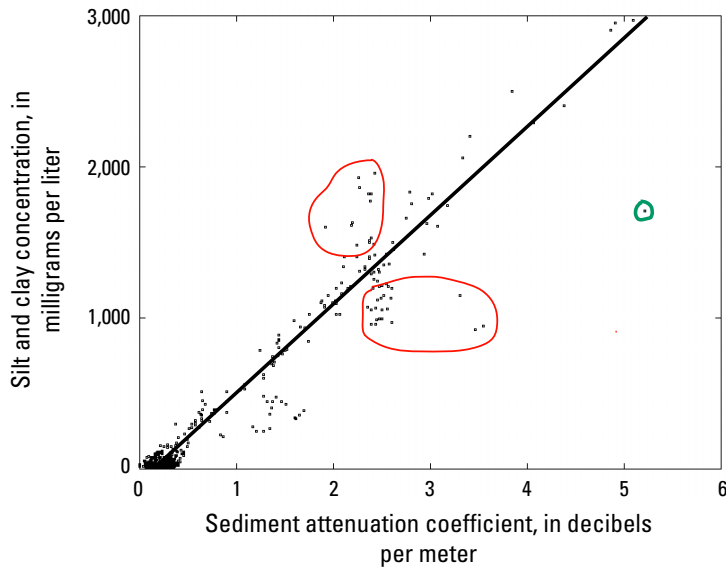


Figure 18. Graph showing relation between the 2-MHz acoustic sediment attenuation coefficient and silt and clay concentration at the CR061 monitoring station. The data circled in red are from the March 2008 controlled-flood experiment, and the data point circled in green is from July 24, 2007. Acoustic sediment attenuation coefficients were calculated from data collected using a 2-MHz Nortek EasyQ acoustic-Doppler profiler.

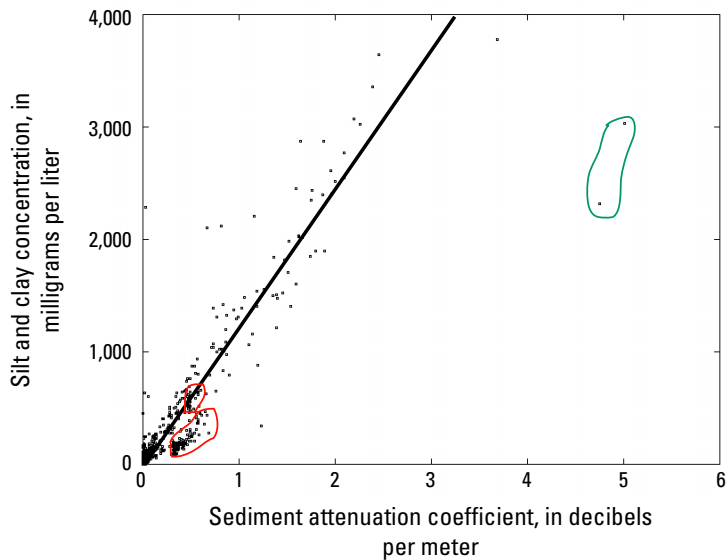


Figure 19. Graph showing relation between the 1-MHz acoustic sediment attenuation coefficient and silt and clay concentration at the CR030 monitoring station. The data circled in red are from the March 2008 controlled-flood experiment, and the data circled in green are from July 24, 2007. Acoustic sediment attenuation coefficients were calculated from data collected using a 1-MHz Nortek EasyQ acoustic-Doppler profiler.

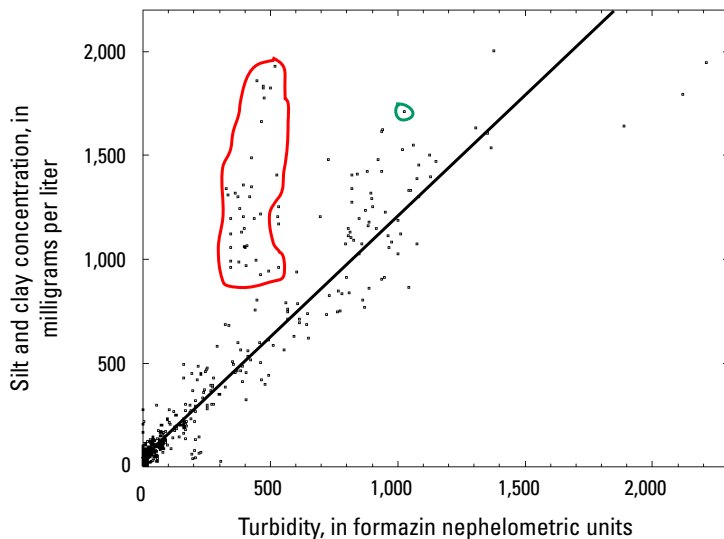


Figure 20. Graph showing relation between turbidity and silt and clay concentration at the CR061 monitoring station. The data circled in red are from the March 2008 controlled-flood experiment, and the data point circled in green is from July 24, 2007.

The apparent data outliers from both of these anomalous events do not arise from errors or mistakes, but rather are explained by changes in the physical properties of the suspended sediment, resulting in a shift in the relations between turbidity, the acoustic sediment attenuation coefficient, and the suspended-sediment concentration. As shown below, with respect to the 2008 controlled-flood-experiment data, these apparent outliers are explained on the basis of grain-size differences, whereas, with respect to the July 2007 data, these outliers can only be explained on the basis of differences other than grain size, specifically color, clay-mineral assemblage, and perhaps increased organic content.

The 2008 controlled-flood experiment was intended to resuspend sand and finer sediment (possibly silt but not likely

clay) from the riverbed for bar building, and accordingly the flood resulted in a much coarser grain-size distribution of suspended silt and clay than is typical for the Colorado River in Grand Canyon. Grain-size distributions of the suspended-sediment samples were measured using two methods, using a Beckman Coulter 13320 particle size analyzer, which measures grain size by laser diffraction, and using the pipet method described by Krumbein and Pettijohn (1938), Poppe and others (2000), and Guy (1969). Using both methods of analysis, the grain-size distribution (fig. 21) was significantly coarser for the 2008 controlled-flood samples (shown in red) than the representative baseline samples (blue) that fall on or near the regression lines shown in figures 18 to 20.

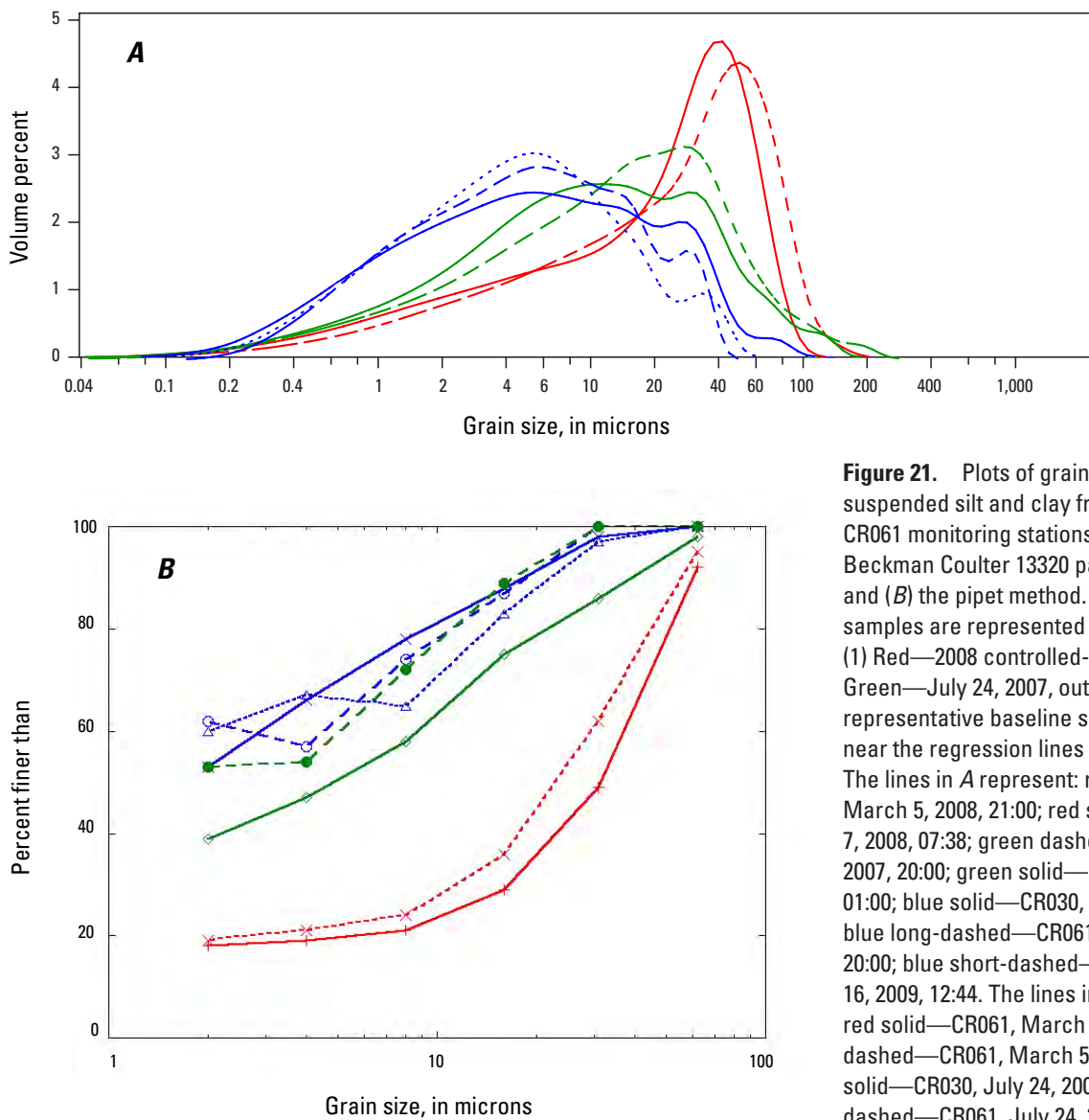


Figure 21. Plots of grain-size distributions of suspended silt and clay from the CR031 and CR061 monitoring stations analyzed using (A) a Beckman Coulter 13320 particle size analyzer and (B) the pipet method. The sediment samples are represented in three categories: (1) Red—2008 controlled-flood experiment; (2) Green—July 24, 2007, outliers; and (3) Blue—representative baseline samples that fall on or near the regression lines (see figs. 18 to 20). The lines in A represent: red dashed—CR061, March 5, 2008, 21:00; red solid—CR061, March 7, 2008, 07:38; green dashed—CR061, July 24, 2007, 20:00; green solid—CR030, July 24, 2007, 01:00; blue solid—CR030, July 26, 2007, 01:00; blue long-dashed—CR061, October 9, 2006, 20:00; blue short-dashed—CR061, September 16, 2009, 12:44. The lines in B represent: red solid—CR061, March 7, 2008, 07:38; red dashed—CR061, March 5, 2008, 21:00; green solid—CR030, July 24, 2007, 01:00; green dashed—CR061, July 24, 2007, 20:00; blue short-dashed—CR030, August 14, 2006, 13:00; blue long-dashed—CR061, October 9, 2006, 20:00; blue solid—CR030, March 3, 2008, 11:44.

Apart from grain size, the physical parameters of the suspended sediment would not be expected to be significantly different during the 2008 controlled-flood experiment when compared with a typical suspended-sediment sample in the study area. This is because the silt and clay transported during the 2008 controlled-flood experiment originated from silt stored in the river bed and in the bars as opposed to new silt and clay being supplied by an upstream tributary. An inspection of silt-and-clay-sized sediment from samples collected during the 2008 controlled-flood experiment through a stereoscopic microscope suggested that the composition of the grains (primarily quartz), grain shape (well rounded), and grain color, at least for the larger grains, did not appear to vary appreciably between the 2008 controlled-flood samples and the baseline samples collected during typical dam releases.

With constant particle composition, both the scattering and absorption components of the attenuation cross-section decrease as grain size increases. The attenuation of light by a particle is the sum of the absorption and scattering of light caused by that particle. The attenuation cross-section of a particle, C , is the attenuation per unit mass concentration, and can be described by the equation

$$C=Q_c s/m, \tag{7}$$

where Q_c is the attenuation efficiency, s is the average projected surface area, and m is the mass of the particle (Davies-Colley and others, 1993). Q_c is nearly constant for light-attenuating mineral particles. Figure 22 shows that for spherical particles made up of quartz, the theoretical attenuation cross-section peaks at a clay-sized particle diameter of approximately 1.6 microns. For particles with a diameter greater than 1.6 microns, the attenuation cross-section decreases as grain size increases (Davies-Colley and others, 1993).

The coarsening of the grain size, and the resulting decrease in the attenuation cross-section, can be related to changes in turbidity, as observed during the March 2008

controlled-flood experiment. The coarser grain-size distribution of the suspended silt and clay observed during the March 2008 controlled-flood experiment compared to baseline conditions (fig. 21) resulted in less scattering of light by the sediment, and consequently lower turbidity, relative to the suspended-silt-and-clay concentration (fig. 20).

The acoustic sediment attenuation coefficient would also be expected to decrease with a coarser grain-size distribution of silt and clay (fig. 6). It is apparent, however, from the results shown in figures 18 through 20 that the change in grain-size distribution of the silt and clay caused by the 2008 controlled-flood experiment had a greater effect on turbidity than on the acoustic sediment attenuation coefficient.

A likely reason why the acoustic sediment attenuation coefficient was not affected as much as turbidity by the coarser grain-size distribution of the silt and clay during the 2008 controlled-flood experiment was that sand-sized particles made up a larger percentage of the total suspended-sediment concentration during the controlled-flood experiment relative to baseline conditions. Figure 23 shows a plot of the 1-MHz acoustic sediment attenuation coefficient at the CR030 station relative to suspended-sediment concentration in different size classes. Under normal dam releases, shown in figure 23A, most of the sediment concentration consists of silt-and-clay-sized particles, in which case the acoustic attenuation occurs primarily through viscous losses (fig. 6). However, the high concentration of sand-sized particles and relatively low concentration of silt-and-clay-sized particles present during the 2008 controlled-flood experiment, shown in figure 23B, likely resulted in a significant amount of acoustic attenuation through scattering losses (fig. 6). Thus, during the 2008 controlled-flood experiment, the expected decrease in acoustic attenuation from viscous losses caused by the coarser particle-size distribution of the silt and clay (fig. 21) was likely offset by a larger contribution to acoustic attenuation from scattering losses caused by an increased concentration of sand-sized particles (fig. 6).

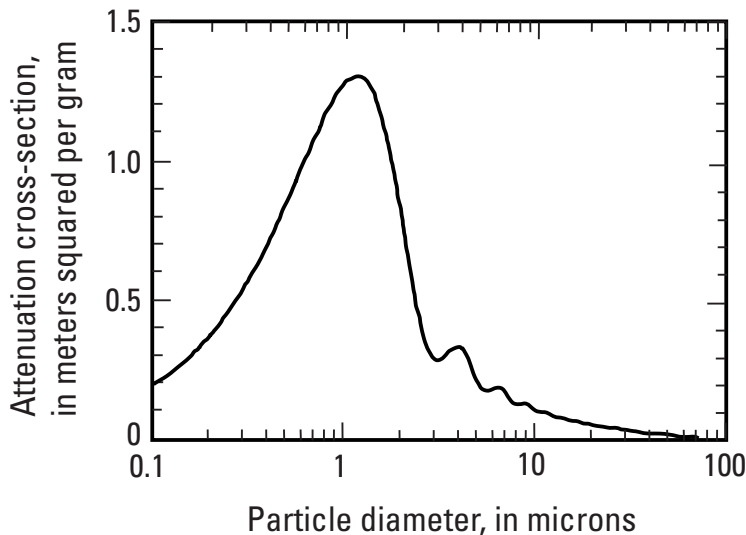


Figure 22. Graph showing the theoretical attenuation cross-section, which is the attenuation of light per unit mass of particles, caused by spherical quartz particles in suspension, as a function of their diameter (modified from Davies-Colley and others, 1993).

EXPLANATION

- Total suspended sediment (sand, silt, and clay)
- Silt and clay
- Sand

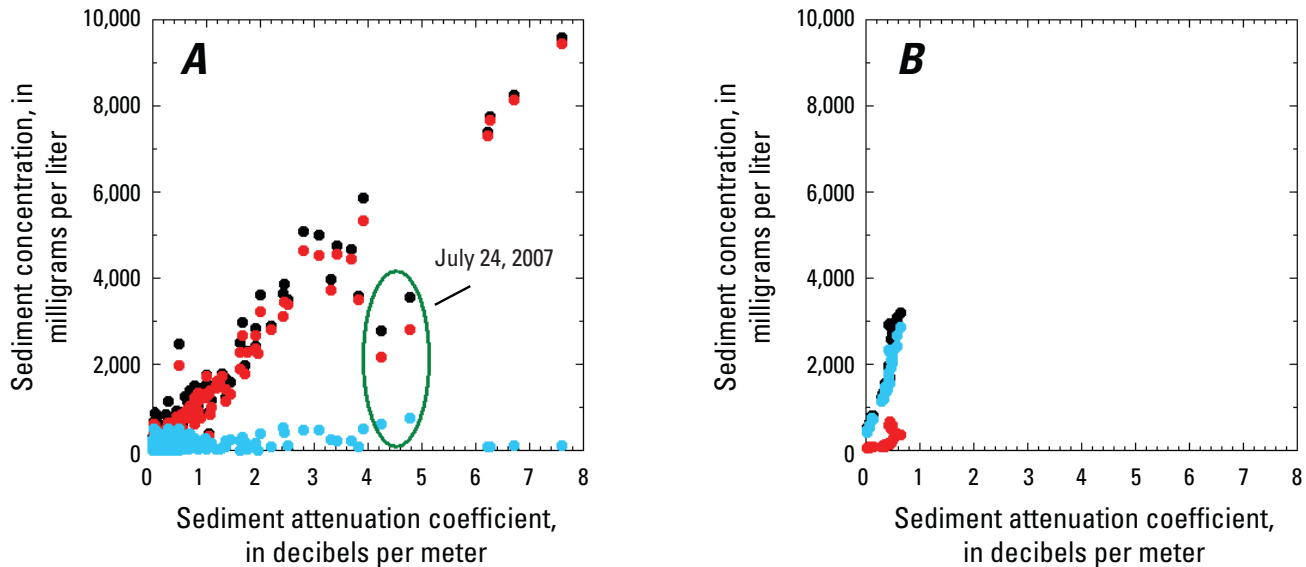


Figure 23. Graphs showing relations between the 1-MHz acoustic sediment attenuation coefficient and sediment concentration in different size classes at the CR030 monitoring station during (A) "normal" dam releases, and (B) the 2008 controlled-flood experiment. Acoustic sediment attenuation coefficients were calculated from data collected using a 1-MHz Nortek EasyQ. Under "normal" dam releases, acoustic attenuation from sediment is mostly the result of silt and clay in the water, as indicated by the fact that the "total sediment" and "silt and clay" data plot nearly on top of one another in A. During the 2008 controlled-flood experiment—when the sand concentrations were typically >1,000 mg/L, the silt and clay was composed mostly of silt (fig. 21), and the silt and clay concentrations were much lower than the sand concentrations—acoustic attenuation from sediment is mostly the result of sand in the water, as expected on the basis of figure 6 and as indicated by the fact that the "total sediment" and "sand" data plot nearly on top of one another in B. The July 24, 2007, apparent outliers in A are circled in green. Data in A are the 806 EWI and calibrated-pump measurements made during November 27, 2004, through March 4, 2008; data in B are the 37 EWI measurements made during March 5–9, 2008 (the pump intake broke during the 2008 controlled-flood experiment, so no pump data could be used for this period).

In contrast to the apparent outliers during the 2008 controlled-flood experiment, the outliers from the anomalous flooding event in July 2007 appear to be caused primarily by changes in the physical properties of the sediment other than a change in the grain-size distribution. It is difficult to determine whether the July 2007 event resulted in low turbidity relative to silt and clay concentration, because there was only one suspended-sediment sample collected during the event when there was measurable turbidity (that is, turbidity below the maximum recording level of the instrument). The single sample collected at the CR061 station on July 24, 2007, appears to have lower turbidity than expected for the silt and clay concentration. As explained earlier, this could be the result of a coarser grain-size distribution; however, it is unclear whether the grain-size distribution of the sample differed from the grain-size distributions of the baseline samples. It appeared to be coarser than the baseline samples from Beckman-Coulter 13320 particle size analyzer laser-diffraction results (fig. 21A, green dash), but showed a similar grain-size distribution as the baseline samples from the pipet method results (fig. 21B, green dash).

Differences in the color of the sediment could play a role in reducing the turbidity during the anomalous flooding event in July 2007, compared to higher baseline turbidity values for similar suspended-silt-and-clay concentrations. Turbidity in the study area was measured using optical instruments with a near infrared (IR) light source, which resulted in measurements that were less sensitive to color change of particles and the dissolved constituents in the water compared with turbidity measurements from instruments with a light source in the visible light wavelength range (Anderson, 2005; Sadar, 2009). Sutherland and others (2000) found that measurements from an optical backscatter sensor, also equipped with a near-IR light source, decreased with increasing blackness level (decreasing Munsell value) of a sample. They found that the scattering efficiency of IR light detected by the optical backscatter sensors was reduced with increasing blackness level of particles because of an increase in the absorption of IR light by the particles, causing major negative interference in turbidity (Sutherland and others, 2000). The main difference between the optical backscatter sensors used in the Sutherland study and the turbidity instruments used in this study is the

orientation of the scattered light that is detected. An optical backscatter sensor detects light scattered back towards the light source, whereas the turbidity instruments used in the Grand Canyon study detect light scattered at 90 degrees (fig. 1). It is reasonable to assume that an increase in blackness level of a sample would also result in reduced scattering efficiency at 90 degrees from the incident light path and thus lower turbidity measured with optical backscatter sensors as well as with the instruments used in the Grand Canyon study. A visual inspection through a stereoscopic microscope of samples from the July 2007 event showed less uniform grains, with a greater percentage of darker and more angular grains than in the baseline samples. Photographs of the samples analyzed for grain-size distribution by the pipet method show the July 24, 2007, samples to be much darker (moderate brown) than the representative baseline or 2008 controlled-flood-experiment samples (light brown or moderate yellowish brown, fig. 24). The silt and clay supplied by House Rock Wash during the large flood on July 23, 2007, and present in the July 24, 2007, suspended-sediment samples collected at the CR030 and CR061 monitoring stations are much darker than the silt and clay supplied by other tributaries and much darker than the silt and clay typically supplied by House Rock Wash. Approximately 10 percent of the House Rock Wash drainage basin was burned during the “Warm Fire” of June 2006 (United States Department of Agriculture Forest Service, 2009), and analyses of data from two stream gages on House Rock Wash (Griffiths and others, 2010) and from a rain-gage network suggest that large amounts of the water and sediment contained in the July 2007 House Rock Wash flood were likely derived from this burn area. Perhaps a combination of an increase in the blackness level of the “burn-derived” sediment with a coarser grain-size distribution resulted in somewhat lower turbidity during the July 2007 event relative to the

silt and clay concentration when compared with the baseline samples (fig. 20).

From figures 18 through 20, the more significant effect of the July 2007 event was an increase in the acoustic sediment attenuation coefficient relative to silt and clay concentration, which is the opposite result expected from the observed coarser grain-size distribution (figs. 6 and 21). The acoustic-sediment-attenuation-coefficient outliers are more significant than the single turbidity outlier, and there is more confidence in their validity because of their consistent positioning relative to the regressions and because they represent three suspended-sediment samples from two sites (CR030 and CR061 stations, figs 18 through 20). Because changes in sediment color cannot affect sound, another physical process must therefore play a role in giving rise to the apparent outliers during the anomalous flooding event in July 2007.

Apart from grain size, irregular grain shape has been shown to result in higher acoustic sediment attenuation (Schaafsma and Hay, 1997). However, the study conducted by Schaafsma and Hay only considered acoustic attenuation caused by scattering (fig. 6). Considering the frequencies of the acoustic instruments and the grain-size distribution, absorption from viscous losses (not scattering losses) is the dominant mechanism of acoustic attenuation in the study area (figs. 6 and 23). Acoustic attenuation from viscous losses increases with increasing total particle surface area, and smaller particles have a greater surface area to volume ratio and thus account for more acoustic (and light) attenuation per mass concentration than larger particles (fig. 6). Irregularly shaped particles have a greater surface area to volume ratio than spherical particles and thus would also be expected to result in increased attenuation by viscous losses per mass concentration. However, the acoustic instruments used in the Grand Canyon study (600 KHz, 1 MHz, and 2 MHz) have

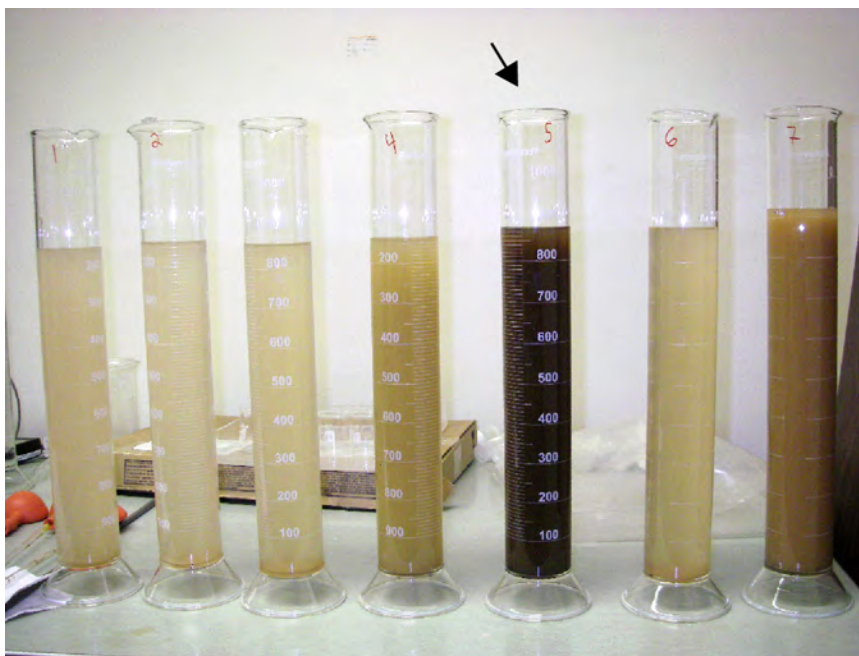


Figure 24. Photograph of sediment samples analyzed for grain-size distribution using the pipet method. The sample marked by the arrow was collected on July 24, 2007, from the CR030 monitoring station. This anomalously dark sample is one of the outliers circled in green in figures 19 and 23 and is depicted as the green solid-line grain-size distribution in figure 21.

long wavelengths relative to the grain sizes being measured; a 1-Mhz frequency instrument emits an acoustic signal with a wavelength of 1.5 millimeters, and grain size of suspended sediment in the study area is dominated by silt and clay less than 63 microns (that is, only about 4 percent as large). This combination of acoustic frequency and particle size satisfies the Rayleigh long wavelength requirement, where there is evidence that particle shape is relatively unimportant, as particles behave as point sources (Dukhin and Goetz, 2002).

The dark color of the silt and clay samples collected on July 24, 2007 (fig. 24), suggests an increase in organic content (primarily ash) derived from areas burned by the Warm Fire. The silt-and-clay-grain-size part of a pump sample from the July 23, 2007, House Rock Wash flood (the likely source of sediment for the July 24, 2007, anomalous event in the study area) was analyzed for organic material by a loss-on-ignition method (Heiri and others, 2001; Veres, 2002). The sample was composed of 9.1 percent by weight of organic material, compared to a sample collected by the pump sampler at the same location previous to the fire, which was composed of 3.7 percent by weight of organic material. Organic content larger than silt-and-clay size was not analyzed from the House Rock Wash pump samples.

With a significantly lower density than the sediment, the organic material would be expected to contribute less to acoustic attenuation through viscous losses than the sediment (Urick, 1948; Thorne and others, 1991). However, the ash in the Colorado River during the July 2007 anomalous event likely made up a significant portion of the volume of material in the river, and perhaps it contributed significantly to acoustic attenuation through a different mechanism than viscous losses, such as thermal losses (Allegra and Hawley, 1972; Dukhin and Goetz, 2002; Guerin and Seaman, 2004). Additionally, if there was a significant contribution of larger organic material (larger than silt size) in suspension during the July 2007 anomalous event, perhaps a significant amount of acoustic attenuation through scattering losses occurred (fig. 6).

The remaining sediment parameter that could affect the acoustic attenuation is particle density (color has no effect on acoustic attenuation, although, as explained earlier, it may help explain a decrease in turbidity during the July 2007 event). As particle density increases (relative to the fluid density), the acoustic attenuation from viscous losses also increases (Urick, 1948; Thorne and others, 1991). Analysis of clay-mineral content using X-ray diffraction (fig. 25; Moore and Reynolds, 1997) suggests that sediment from the July 24, 2007, anomalous event was similar to sediment from the July 23, 2007, House Rock Wash flood and was composed of an assemblage of denser clay minerals than was present in baseline samples. The two baseline samples that were analyzed for clay-mineral content are represented in figures 18 through 20 by data points that plot near the regression lines. The CR030 station July 24, 2007, sample and House Rock Wash July 23, 2007, sample contained a lower percentage of smectite, which has a lower wet density (1.8 g/cm^3) than the other two clay minerals present in the samples, illite (2.1 g/cm^3) and kaolinite (2.4 g/cm^3 ;

De Wit and Arens, 1950). Because these samples contained less smectite, their clay assemblages were denser than those of the other samples that were analyzed. The August 2003 House Rock Wash sample, preceding the 2006 Warm Fire, had a clay assemblage more similar to the Paria River sample than to the post-fire House Rock Wash sample. The X-ray diffraction results provide additional evidence (albeit from a small sample size) that the Warm Fire exposed new material to erosion, specifically upland sediment from the Kaibab plateau (United States Department of Agriculture Forest Service, 2009; Billingsley and Priest, 2010), which resulted in a provenance not previously observed for sediment entering the Colorado River. The denser sediment (particularly clay), combined with an increase in organic material (primarily ash and other burned organic material) in the river, were possibly responsible for the abnormally high acoustic attenuation during the July 2007 anomalous event. These analyses together illustrate that apparent data outliers in plots of acoustic sediment attenuation coefficient vs. turbidity, silt and clay concentration vs. acoustic sediment attenuation coefficient, and silt and clay concentration vs. turbidity can be used to deduce sediment provenance.

Conclusion

Depending on the design parameters of the instrument, turbidity is dependent to different degrees on the physical parameters of the sediment in the water, particularly concentration, grain size, grain shape, and color. Thus, different models of turbidity instruments measure turbidity differently, even when manufacturers report the data in the same units of measurement. This issue makes it difficult to compare turbidity between rivers when different instruments are used. Turbidity instruments also have a limited measurement range of sediment concentration, which is also dependent on instrument design. Because of these instrument characteristics, turbidity is of limited use as a surrogate for suspended-sediment concentration when grain size and sediment composition vary greatly, and also under conditions of high sediment concentration. In the Colorado River in Grand Canyon, multifrequency arrays of acoustic instruments have proven to be more useful than turbidity as a surrogate for suspended-sediment concentration. The multifrequency arrays of acoustic instruments are unaffected by sediment color and are better able to compensate for the variability of the other characteristics of suspended sediment, except for large changes in clay-mineral content. Also, the acoustic instruments are able to measure the entire range of suspended-sediment concentration that occurs in the study area.

Turbidity is nonetheless a valuable measure of visual clarity in rivers when related to biological processes that are controlled by light availability, such as predator-prey interactions among fish and food production for aquatic organisms (gross primary productivity). For example, visual clarity of the Colorado River has been linked to food availability for fish

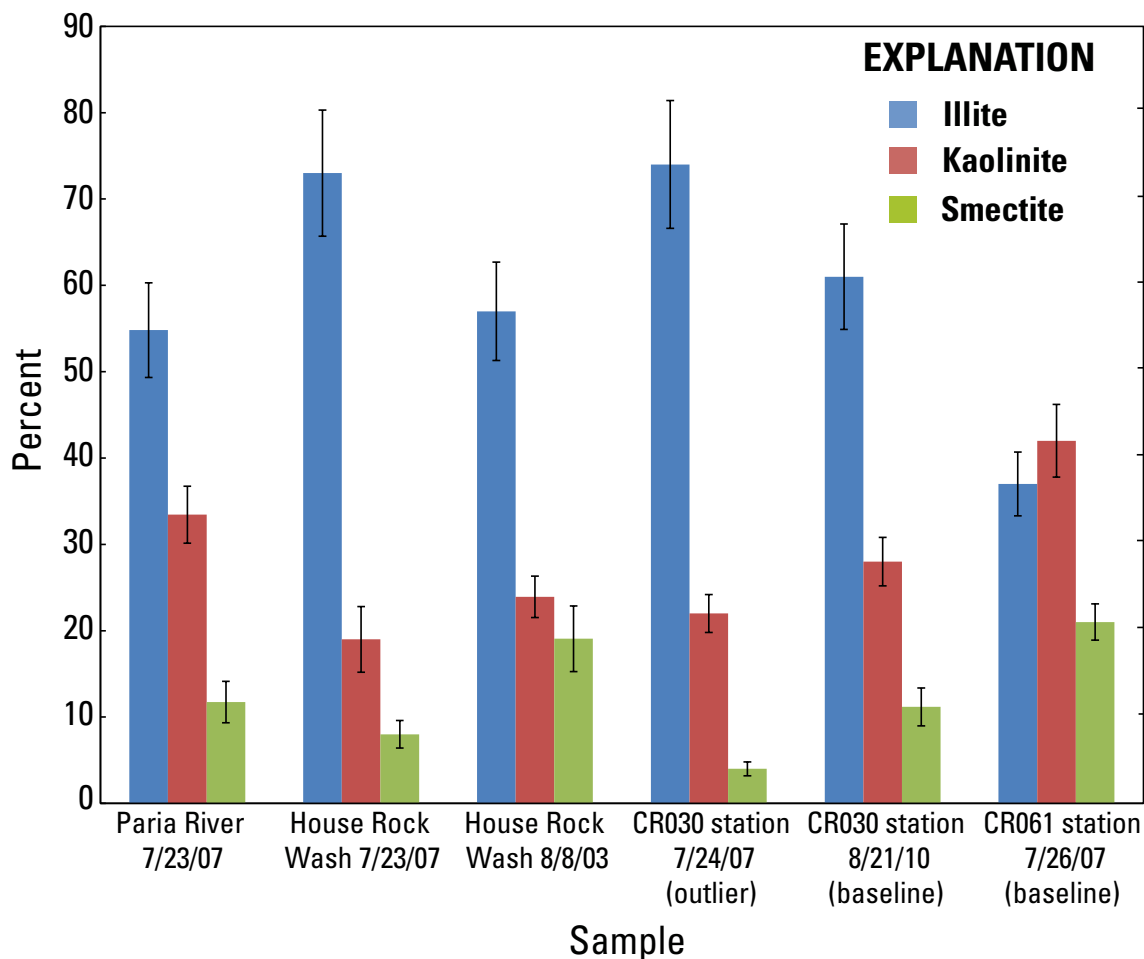


Figure 25. Bar graph of clay mineral assemblages in suspended-sediment samples determined by x-ray diffraction. Suspended sediment from the CR030 station on July 24, 2007, likely came from House Rock Wash on July 23, 2007. The July 24, 2007, CR030 station sample is one of the outliers circled in green in figure 19, whereas the two samples labeled 'baseline' in the bar graph are represented in figures 18 through 20 as data points near the regression lines. The error bars shown in the bar graph are ± 10 percent of the values of clay minerals that make up at least 20 percent of the total percentage of clay minerals and ± 20 percent of the values of clay minerals that make up less than 20 percent of the total (Moore and Reynolds, 1997).

and to salmonid feeding behavior (and ultimately salmonid health). Thus, visual clarity of the Colorado River is likely a factor in determining the extent that salmonids actively feed on fish (Yard and others, 2011) and may also influence whether salmonids move into and out of areas where native humpback chub exist. Visual clarity in the study area is primarily influenced by silt and clay influx into the Colorado River. However, because of the variability of the sediment characteristics in the study area, particularly grain size distribution, turbidity is a better indicator of visual clarity than suspended-sediment concentration.

Clear water conditions exist most of the time in the study area, interrupted by periods of low visual clarity resulting from tributary flooding during summer and fall thunderstorms. Turbidity during these runoff events is frequently above the maximum recording level of the probes, and to determine the relevance of turbidity to biological processes affected by visual clarity, it is necessary to estimate this unmeasurable turbidity. The turbidity record above the maximum recording

level of the probes was derived in the study area by using a relation between turbidity and the acoustic sediment attenuation coefficient. Turbidity was estimated before the construction of Glen Canyon Dam (when turbidity data were sparse) based on the relation between turbidity and suspended-silt-and-clay concentration. These pre-dam turbidity estimates were higher than post-dam turbidity by an average of a factor of approximately 2,000 at the upstream CRLF station. Continuous monitoring of turbidity and comparison with pre-dam conditions are necessary to evaluate the effects of sediment influx and dam operations on biological processes affected by visual clarity.

By comparing turbidity with acoustic-Doppler profiler data and suspended-sediment concentration, this study identified and investigated rare sediment inputs with unusual physical properties. The two examples examined in the study were (1) a controlled-flood experiment, which resulted in a substantial increase in grain size of suspended sediment and was responsible for abnormally low turbidity relative to

suspended-sediment concentration, and (2) a tributary flood in a watershed altered by a major wildfire, which resulted in both an increase in organic material entering the study area and an increase in suspended sediment that was composed of an assemblage of abnormally dense clay minerals. The higher concentration of organics (primarily ash and other combusted material) and the higher density of the clay minerals brought into the study area from the tributary flood may have been the cause of the abnormally high acoustic attenuation (relative to suspended-sediment concentration) in the study area. Identifying these atypical sediment inputs, as well as the physical properties that differentiate them from the “typical” suspended sediment in the system, provides information defining the range and influence of various sources of sediment in the study area. Apart from providing a better understanding of sediment provenance in a watershed, this information could, in some study areas, provide other valuable information, such as identification of potential sources of pollution associated with different sources of sediment.

References Cited

- Abrahams, M., and Kattenfeld, M., 1997, The role of turbidity as a constraint on predator-prey interactions in aquatic environments: *Behavioral Ecology and Sociobiology*, v. 40, p. 169–174, available online at <http://www.jstor.org/stable/4601315>.
- Agrawal, Y.C., and Pottsmith, H.C., 2000, Instruments for particle size and settling velocity observations in sediment transport: *Marine Geology*, v. 168, p. 89–114.
- Agrawal, Y.C., Whitmire, A., Mikkelsen, O.A., and Pottsmith, H.C., 2008, Light scattering by random shaped particles and consequences on measuring suspended sediments by laser diffraction: *Journal of Geophysical Research*, v. 113, C04023, accessed online at <http://www.agu.org/pubs/crossref/2008/2007JC004403.shtml>.
- Aksnes, D.L., and Giske, J., 1993, A theoretical model of aquatic visual feeding: *Ecological Modeling*, v. 67, p. 233–250.
- Allegra, J.R., and Hawley, S.A., 1972, Attenuation of sound in suspensions and emulsions; theory and experiments: *Journal of the Acoustical Society of America*, v. 51, p. 1545–1564.
- American Public Health Association, American Water Works Association, and Water Pollution Control Federation, 2005, *Standard methods for the examination of water and wastewater* (21st ed.): Washington, D.C., American Public Health Association, 1,200 p.
- Anderson, C.W., 2005, Turbidity: U.S. Geological Survey *Techniques of Water-Resources Investigations*, book 9, chapter A6.7, accessed online at <http://pubs.water.usgs.gov/twri9A>.
- ASTM International, 2011, *Standard guide for the use of various turbidimeter technologies for measurement of turbidity in water*: Conshohocken, Pa., West ASTM International, D7726-11, 17 p.
- Beverage, J.P., and Culbertson, J.K., 1964, Hyperconcentrations of suspended sediment: *Journal of Hydraulics Division*, American Society of Civil Engineers, v. 90, no. 6, p. 117–128.
- Billingsley, G.H., and Priest, S.S., 2010, Geologic map of the House Rock Valley area, Coconino County, Northern Arizona: U.S. Geological Survey Scientific Investigations Map 3108, available online at <http://pubs.usgs.gov/sim/3108/>.
- Blanchard, S.F., and Schertz, T.L., 2009, *Publication of Techniques and Methods Report Book 3, Chapter C4, Guidelines and procedures for computing time-series suspended-sediment concentrations and loads from in-stream turbidity-sensor and streamflow data*, by Patrick P. Rasmussen, John R. Gray, G. Douglas Glysson, and Andrew C. Ziegler: U.S. Geological Survey Office of Surface Water and Office of Water Quality Joint Technical Memorandum, 2010.01 and 2010.04, accessed online at <http://water.usgs.gov/admin/memo/QW/qw10.04.html>.
- Breusch, T.S., and Pagan, A.R., 1979, A simple test for heteroscedasticity and random coefficient variation: *Econometrica*, v. 47, p. 1287–1294.
- Christensen, V.G., Rasmussen, P.P., and Ziegler, A.C., 2002, Comparison of estimated sediment loads using continuous turbidity measurements and regression analysis: *Turbidity and Other Surrogates Workshop*, Reno, Nevada, April 30–May 2, 2002, Proceedings, accessed online at <http://water.usgs.gov/osw/techniques/TSS/christensen.pdf>.
- Davies-Colley, R.J., Smith, D.G., and Vant, W.N., 1993, *Colour and clarity of natural waters; science and management of optical water quality*: London, Ellis Horwood, 310 p.
- De Wit, C.T., and Arens, P.L., 1950, Moisture content and density of some clay minerals and some remarks on the hydration pattern of clay: *Transactions of the International Congress of Soil Science*, Amsterdam 1950, v. 2, p. 59–62.
- Dukhin, A.S., and Goetz, P.J., 2002, *Ultrasound for characterizing colloids—particle sizing, zeta potential, rheology*: The Netherlands, Elsevier, 372 p.
- Edwards, T.K., and Glysson, G.D., 1999, Field methods for measurement of fluvial sediment: U.S. Geological Survey *Techniques of Water-Resources Investigations*, book 3, chapter C2, 89 p., available online at <http://pubs.usgs.gov/twri/twri3-c2/>.
- Finlayson, B. L., 1985, Field calibration of a recording turbidity meter: *Catena*, v. 12, p. 141–147.
- Flammer, G.H., 1962, *Ultrasonic measurement of suspended sediment*: U.S. Geological Survey Bulletin 114-A, 48 p.

- Gartner, J.W., 2004, Estimating suspended solids concentrations from backscatter intensity measured by acoustic Doppler current profiler in San Francisco Bay, California: *Marine Geology*, v. 211, p. 169–187.
- Gilvear, D.J., and Petts, G.E., 1985, Turbidity and suspended solids variations downstream of a regulating reservoir: *Earth Surface Processes and Landforms*, v. 10, p. 363–373.
- Gippel, C.J., 1989, The use of turbidimeters in suspended sediment research: *Hydrobiologia*, v. 176, no. 177, p. 465–480.
- Gorman, O.T., and Stone, D.M., 1999, Ecology of spawning humpback chub, *Gila cypha*, in the Little Colorado River near Grand Canyon, Arizona: *Environmental Biology of Fishes*, v. 55, p. 115–133.
- Grams, P.E., and Schmidt, J.C., 2005, Equilibrium or indeterminate? Where sediment budgets fail; sediment mass balance and adjustment of channel form, Green River downstream from Flaming Gorge Dam, Utah and Colorado: *Geomorphology*, v. 71, p. 156–181.
- Gray, J.R., and Simoes, F.J.M., 2008, Estimating sediment discharge, appendix D in Garcia, M.H., ed., *Sedimentation engineering—processes, measurements, modeling, and practice: American Society of Civil Engineers Manuals and Reports on Engineering Practice No. 110*, p. 1067–1088.
- Gregory, R.S., 1993, Effect of turbidity on the predator avoidance behaviour of juvenile Chinook salmon (*Oncorhynchus tshawytscha*): *Canadian Journal of Fisheries and Aquatic Sciences*, v. 50, p. 241–246.
- Griffiths, R.E., Topping, D.J., Andrews, T., Bennett, G.E., Sabol, T.A., and Melis, T.S., 2012, Design and maintenance of a network for collecting high-resolution suspended-sediment data at remote locations on rivers, with examples from the Colorado River: *U.S. Geological Survey Techniques and Methods*, book 8, chapter C2, 44 p., accessed online at <http://pubs.usgs.gov/tm/tm8c2/>.
- Griffiths, R.E., Topping, D.J., McDonald, R.R., and Sabol, T.A., 2010, The use of the multi-dimensional surface-water modeling system (MD_SWMS) in calculating discharge and sediment transport in remote ephemeral streams: Second Joint Federal Interagency Conference on Sedimentation and Hydrologic Modeling, Las Vegas, Nev., June 27–July 1, 2010, Proceedings, accessed online at http://acwi.gov/sos/pubs/2ndJFIC/Contents/P40_Griffiths_paper.pdf.
- Guerin, M., and Seaman, J.C., 2004, Characterizing clay mineral suspensions using acoustic and electroacoustic spectroscopy—a review: *Clays and Clay Minerals*, v. 52, p. 145–157, available online at <http://cm.geoscienceworld.org/content/52/2/145.full.pdf>.
- Guy, H.P., 1969, Laboratory theory and methods for sediment analysis: *U.S. Geological Survey Techniques of Water-Resources Investigations*, book 5, chapter C1, 58 p., available online at <http://pubs.usgs.gov/twri/twri5c1/>.
- Hach, C.C., Vanous, R.D., and Heer, J.M., 1985, Understanding turbidity measurements: Hach Company, Technical Information Series-Booklet No. 11 (1st ed.), 11 p.
- Heiri, O., Lotter, A.F., and Lemcke, G., 2001, Loss-on-ignition as a method for estimating organic and carbonate content in sediments; reproducibility and comparability of results: *Journal of Paleolimnology*, v. 25, p. 101–110.
- Helsel, D.R., and Hirsch, R.M., 2002, Statistical methods in water resources: *U.S. Geological Survey Techniques of Water-Resources Investigations*, book 4, chapter A3, 522 p., accessed online at <http://pubs.usgs.gov/twri/twri4a3/>.
- Kirk, J.T.O., 1985, Effects of suspensoids (turbidity) on penetration of solar radiation in aquatic systems: *Hydrobiologia*, v. 125, p. 195–208, available online at <http://link.springer.com/article/10.1007%2FBF00045935#page-1>.
- Krumbein, W.C., and Pettijohn, F.J., 1938, *Manual of sedimentary petrography*: New York, Appleton-Century-Crofts, 549 p.
- Lewis, J., 1996, Turbidity-controlled suspended sediment sampling for runoff-event load estimation: *Water Resources Research*, v. 32, no. 7, p. 2299–2310, available online at <http://www.fs.fed.us/psw/publications/lewis/Lewis96.pdf>.
- Lohrmann, A., 2001, Monitoring sediment concentration with acoustic backscattering instruments: Nortek Technical Note No. 3, 5 p., available online at <http://www.nortekusa.com/lib/technical-notes/seditments>.
- Melis, T.S., Topping, D.J., and Rubin, D.M., 2003, Testing laser-based sensors for continuous in situ monitoring of suspended sediment in the Colorado River, Arizona, in Bogen, J., Fergus, T., and Walling, D.E., eds., *Erosion and sediment transport measurement in rivers; technological and methodological advances*: Wallingford, U.K., IAHS Press, International Association of Hydrological Sciences Publication 283, p. 21–27.
- Moore, D.M., and Reynolds, R.C., Jr., 1997, *X-ray diffraction and the identification and analysis of clay minerals* (2d ed.): Oxford, Oxford University Press, 378 p.
- Poppe, L.J., Eliason, A.H., Fredericks, J.J., Rendigs, R.R., Blackwood, D., and Polloni, C.F., 2000, Grain-size analysis of marine sediments—methodology and data processing, chap. 1 of *USGS East-Coast sediment analysis; procedures, database, and georeferenced displays*: U.S. Geological Survey Open-File Report 00-358, accessed online at <http://pubs.usgs.gov/of/of00-358/text/contents.htm>.

- Porterfield, G., 1972, Computation of fluvial-sediment discharge: U.S. Geological Survey Techniques of Water Resources Investigations, book 3, chapter C3, 66 p., available online at <http://pubs.usgs.gov/twri/twri3-c3/>.
- Rantz, S.E., and others, 1982, Measurement and computation of streamflow—Volume 2, Computation of discharge: U.S. Geological Survey Water-Supply Paper 2175, p. 285–631, available online at <http://pubs.usgs.gov/wsp/wsp2175>.
- Rasmussen, P.P., Gray, J.R., Glysson, G.D., and Ziegler, A.C., 2009, Guidelines and procedures for computing time-series suspended-sediment concentrations and loads from in-stream turbidity-sensor and streamflow data: U.S. Geological Survey Techniques and Methods, book 3, chapter C4, 53 p., accessed online at <http://pubs.usgs.gov/tm/tm3c4/>.
- Sadar, M.J., 1998, Turbidity science: Loveland, Colo., Hach Company, Technical Information Series, Booklet No. 11, 26 p.
- Sadar, M.J., 2009, The basics of turbidity measurement technologies: Prepared for the Methods and Data Comparability Board QA/QC Sensors Group, 12 p., accessed online at http://www.watersensors.org/files/Turbidimeter_Summary.pdf.
- Schaafsma, A.S., and Hay, A.E., 1997, Attenuation in suspensions of irregularly shaped sediment particles—A two-parameter equivalent spherical scatterer model: *Journal of the Acoustical Society of America*, v. 83, p. 598–610.
- Schmidt, E.W., 1984, Hydrazine and its derivatives; preparation, properties, applications: New York, John Wiley and Sons, 1,059 p.
- Schmidt, J.C., and Grams, P.E., 2011a, The high flows—physical science results, in Melis, T.S., ed., Effects of three high-flow experiments on the Colorado River ecosystem downstream from Glen Canyon Dam, Arizona: U.S. Geological Survey Circular 1366, p. 53-91, accessed online at <http://pubs.usgs.gov/circ/1366/>.
- Schmidt, J.C., and Grams, P.E., 2011b, Understanding physical processes of the Colorado River, in Melis, T.S., ed., Effects of three high-flow experiments on the Colorado River ecosystem downstream from Glen Canyon Dam, Arizona: U.S. Geological Survey Circular 1366, p. 17-51, accessed online at <http://pubs.usgs.gov/circ/1366/>.
- Stone, D.M., 2010, Overriding effects of species-specific turbidity thresholds on hoop-net catch rates of native fishes in the Little Colorado River, Arizona: *Transactions of the American Fisheries Society*, v. 139, no. 4, p. 1150–1170, available online at <http://www.tandfonline.com/doi/pdf/10.1577/T09-038.1>.
- Sutherland, T.F., Lane, P.M., Amos, C.L., and Downing, J., 2000, The calibration of optical backscatter sensors for suspended sediment of varying darkness levels: *Marine Geology*, v. 162, p. 587–597.
- Thorne, P.D., and Campbell, S.C., 1992, Backscattering by a suspension of spheres: *Journal of the Acoustical Society of America*, v. 92, no. 2, p. 978–986.
- Thorne, P.D., and Hanes, D.M., 2002, A review of acoustic measurements of small-scale sediment processes: *Continental Shelf Research*, v. 22, p. 603–632.
- Thorne, P.D., Hardcastle, P.J., and Soulsby, R.L., 1993, Analysis of acoustic measurements of suspended sediments: *Journal of Geophysical Research*, v. 98, n. C1, p. 899–910.
- Thorne, P.D., Vincent, C.E., Hardcastle, P.J., Rehman, S., and Pearson, N., 1991, Measuring suspended sediment concentration using acoustic backscatter devices: *Marine Geology*, v. 98, p. 7–16, available online at <http://www.sciencedirect.com/science/article/pii/002532279190031X#>.
- Topping, D.J., Melis, T.S., Rubin, D.M., and Wright, S.A., 2004, High-resolution monitoring of suspended-sediment concentration and grain size in the Colorado River in Grand Canyon using a laser-acoustic system, in Hu, C., and Tan, Y., eds., *International Symposium on River Sedimentation, 9th, Yichang, People's Republic of China, 2004, Proceedings*, p. 2507–2514, accessed online at http://www.gemrc.gov/library/reports/Physical/Fine_Sed/Topping2004.pdf.
- Topping, D.J., Rubin, D.M., Grams, P.E., Griffiths, R.E., Sabol, T.A., Voichick, N., Tusso, R.B., Vanaman, K.M., and McDonald, R.R., 2010, Sediment transport during three controlled-flood experiments on the Colorado River downstream from Glen Canyon Dam, with implications for eddy-sandbar deposition in Grand Canyon National Park: U.S. Geological Survey Open-File Report 2010–1128, 111 p., accessed online at <http://pubs.usgs.gov/of/2010/1128/>.
- Topping, D.J., Rubin D.M., Nelson, J.M., Kinsel, P.J., III, and Corson, I.C., 2000b, Colorado River sediment transport 2. Systematic bed-elevation and grain-size effects of sand supply limitation: *Water Resources Research*, v. 36, p. 543–570, available online at <http://onlinelibrary.wiley.com/doi/10.1029/1999WR900286/pdf>.
- Topping, D.J., Rubin, D.M., and Vierra, L.E., Jr., 2000a, Colorado River sediment transport 1. Natural sediment supply limitation and the influence of Glen Canyon Dam: *Water Resources Research*, v. 36, p. 515–542, available online at <http://onlinelibrary.wiley.com/doi/10.1029/1999WR900285/pdf>.
- Topping, D.J., Wright, S.A., Melis, T.S., and Rubin, D.M., 2006, High-resolution monitoring of suspended-sediment concentration and grain size in the Colorado River using laser-diffraction instruments and a three-frequency acoustic system: 8th Federal Inter-Agency Sedimentation Conference, Reno, Nevada, April 2-6, 2006, Proceedings (CD-ROM), ISBN 0-9779007-1-1, available online at http://www.usbr.gov/uc/rm/amp/twg/mtgs/06may24/Attach_03g.pdf.

- Topping, D.J., Wright, S.A., Melis, T.S., and Rubin, D.M., 2007, High-resolution measurements of suspended-sediment concentration and grain size in the Colorado River in Grand Canyon using a multi-frequency acoustic system: Tenth International Symposium on River Sedimentation, Moscow, Russia, August 1–4, 2007, Proceedings, p. 330–339, ISBN 978-5-89575-124-4, 978-5-89575-127-5, available online at <http://www.riversimulator.org/Resources/GCMRC/PhysicalResources2/Topping2007b.pdf>.
- United States Department of Agriculture Forest Service, 2009, Final Environmental Impact Statement from the Warm Fire Recovery Project, Kaibab National Forest, Coconino County, Arizona: United States Department of Agriculture Forest Service, 315 p., accessed online at http://www.fs.usda.gov/Internet/FSE_DOCUMENTS/stelprdb5138681.pdf.
- Urick, R.J., 1948, The absorption of sound in suspensions of irregular particles: *Journal of the Acoustical Society of America*, v. 20, no. 3, p. 283–289.
- Urick, R.J., 1975, *Principles of underwater sound for engineers*: New York, McGraw-Hill, 384 p.
- Veres, D.S., 2002, A comparative study between loss on ignition and total carbon analysis on mineralogic sediments: *Studia Universitatis Babeş-Bolyai, Geologia*, v. 47, no. 1, p. 171–182.
- Voichick, N., 2008, Specific conductance in the Colorado River between Glen Canyon Dam and Diamond Creek, northern Arizona, 1988–2007: U.S. Geological Survey Data Series 364, 16 p., accessed online at <http://pubs.usgs.gov/ds/364/ds364.pdf>.
- Voichick, N., and Topping, D.J., 2010, Use of specific conductance in estimating salinity and as a natural tracer of water parcels in the Colorado River between Glen Canyon Dam and Diamond Creek, northern Arizona, *in* Proceedings of the Colorado River Basin Science and Resource Management Symposium, November 18–20, 2008, Scottsdale, Arizona: U.S. Geological Survey Scientific Investigations Report 2010–5135, p. 357–362, available online at <http://pubs.usgs.gov/sir/2010/5135/>.
- Voichick, N., and Wright, S.A., 2007, Water-temperature data for the Colorado River and tributaries between Glen Canyon Dam and Spencer Canyon, northern Arizona, 1988–2005: U.S. Geological Survey Data Series 251, 24 p., accessed online at <http://pubs.usgs.gov/ds/2007/251/>.
- Wagner, R.J., Boulger, R.W., Jr., Oblinger, C.J., and Smith, B.A., 2006, Guidelines and standard procedures for continuous water-quality monitors—station operation, record computation, and data reporting: U.S. Geological Survey Techniques and Methods, book 1, chapter D3, 51 p., 8 attachments, available online at <http://pubs.water.usgs.gov/tm1d3>.
- Wall, G.R., Nystrom, E.A., and Litten, S., 2006, Use of an ADCP to compute suspended-sediment discharge in the tidal Hudson River, New York: U.S. Geological Survey Scientific Investigations Report 2006–5055, 16 p.
- Wright, S.A., Anderson, C.R., and Voichick, N., 2008, A simplified water temperature model for the Colorado River below Glen Canyon Dam: *River Research and Applications*, v. 25, no. 6, p. 675–686, accessed online at <http://onlinelibrary.wiley.com/doi/10.1002/rra.1179/pdf>.
- Wright, S.A., Topping, D.J., and Williams, C.A., 2010, Discriminating silt-and-clay from suspended-sand in rivers using side-looking acoustic profilers: Second Joint Federal Interagency Conference on Sedimentation and Hydrologic Modeling, Las Vegas, Nev., June 27–July 1, 2010, Proceedings, accessed online at http://acwi.gov/sos/pubs/2ndJFIC/Contents/2C_Wright_03_01_10_paper.pdf.
- Yard, M.D., Coggins, L.G., Baxter, C.V., Bennett, G.E., and Korman, J., 2011, Piscivory in the Colorado River, Grand Canyon; effects of turbidity, temperature, and fish prey availability: *Transactions of the American Fisheries Society*, v. 140, no. 2, p. 471–486, accessed online at <http://www.tandfonline.com/doi/pdf/10.1080/00028487.2011.572011>.
- YSI Incorporated, 2002, 6-Series operations manual, Item no. 069300, Rev. B, Appendix E.
- YSI Incorporated, 2005, Reconciling 6026 and 6136 turbidity data: Technical Note 0302 T615, 1 p., accessed online at <http://www.ysi.com/media/pdfs/T615-Reconciling-6026-and-6136-Turbidity-Data.pdf>.

